SCINTILLATION AND MAGNETIC SPECTROMETER STUDIES OF NUCLEAR REACTIONS

Thesis by

Ralph W. Kavanagh

In Partial Fulfillment of the Requirements

For the Degree of

Doctor of Philosophy

California Institute of Technology

Pasadena, California

1956

ACKNOWLEDGMENTS

The author is grateful for much helpful criticism and advice from Professors C. C. Lauritsen, W. A. Fowler, R. F. Christy, T. Lauritsen, and W. Whaling during the course of these experiments. Copious assistance was also given by Dr. R. Sherr and by Dr. C. A. Barnes and is appreciated very much. The assistance of Mr. W. R. Mills with the magnetic-lens spectrometer measurements is gratefully acknowledged.

This work was supported by the Office of Naval Research and the Atomic Energy Commission.

ABSTRACT

1. The reaction $Mg^{25}(p,\gamma)Al^{26}(\beta^+)Mg^{26}$ has been examined with a scintillation spectrometer and with a magnetic-lens spectrometer for proton energies from 670 to 1220 kev. The beta and gamma spectra and gamma-gamma coincidences are used with the shell model to assign spins to the low-lying states of Al^{26}; the positron-emitter is found to be an isomeric state at 219 kev excitation.

2. Gamma and alpha emission from the lowest T = 1 state in C^{12} at 15.1 Mev are compared, and an upper limit of 0.1 kev is inferred for the width of the state, using results from deuteron bombardment of boron targets. The cross section for production of the gamma ray is given for deuteron energies from 1.633 Mev (threshold) to 3.25 Mev. Using the $B^{11}(d,p)B^{12}$ reaction, a 1.3 $^{o}/_{o}$ branching of the B^{12} beta decay to the 4.43-Mev state of C^{12} has been found by beta-gamma coincidences, indicating $J = 1^+$ for the lowest T = 1 triad.

TABLE OF CONTENTS

I. INTRODUCTION

In common with most work in the field of nuclear spectroscopy, the purpose of the investigations described in this thesis has been to determine the energies, spins, and parities of certain nuclear energy eigenstates. For the determination of spins (and parities) the direct method of measurement of angular distributions of reaction products has not been available in the present cases. It has been found possible, however, to make assignments in B^{12}, C^{12}, and Al^{26} by inference from this and other work, in conjunction with shell-model hypotheses and the charge-independence of nuclear forces.

The reactions which were studied were produced by the proton bombardment of magnesium targets and the deuteron bombardment of boron targets. The energetic particles were accelerated in either the 2-Mev or the 3-Mev Van de Graaff generator of the Kellogg Radiation Laboratory and analyzed magnetically or electrostatically to 0.2 - 0.3 percent in momentum or energy, respectively, with the aid of collimating slits placed before the target chambers. Beam currents ranged from 0.2 to 2 microamperes, and the total charge per run was determined by current integration accurate to a few percent. Targets were maintained at +300 volts with respect to surroundings and a guard ring at -300 volts around the beam isolated the target chamber from the up-beam slits, such precautions being taken to prevent secondary electrons from interfering with current measurement. Apparatus for the detection of target emanations will be considered in later sections.

II. THE REACTION $Mg^{25}(p, \gamma)Al^{26}(\beta^+)Mg^{26}$

A. BACKGROUND

At the time this work was initiated, there existed a considerable amount of contradictory evidence about the low-lying states of Al^{26}, most of which has been summarized by Endt and Kluyver[1] in a review article. The empirical ground-state mass defect (mass minus mass number) ranged over values from -6.0 ± 0.1 Mev (by $Mg^{25}(d, n)$ neutron groups) to -3.6 ± 0.4 Mev (by $Al^{27}(\gamma, n)$ threshold). Values for the maximum energy of the positron decay to Mg^{26}, determined by absorption techniques and by cloud chamber, had a spread of 600 kev, and the value of 2.8 Mev adopted by Endt and Kluyver was 400 kev under the present well-known value of 3.20 Mev. Work with natural magnesium targets (78.6 $^{o}/_{o}$ Mg^{24}, 10.1 $^{o}/_{o}$ Mg^{25}, and 11.3 $^{o}/_{o}$ Mg^{26}) was complicated by the fact that Al^{25} and Al^{26} have very nearly the same end-point energies[2] ($E_{\beta}(max) = 3.28$ Mev for Al^{25}) and similar half-lives[3] (6.6 seconds for Al^{26} and 7.6 seconds for Al^{25}). The ft-values, to be discussed more fully later, put these transitions in the allowed (favored) class, the expected results for the Al^{25} - Mg^{25} mirror transition. This fact, coupled with the $J = 0^+$ ground state[1] of Mg^{26}, established the spin of the 6.6-second state of Al^{26} as 0^+ or 1^+.

The early $Mg^{25}(d, n)$ and beta decay data were taken by Stahelin[4] to indicate that the beta decay proceeded from an isomeric state of Al^{26} about 2 Mev above the ground state. Since he found no indication of a gamma transition accompanying the positrons,[4, 5] the assignments

$J = 0^+$ and $J = 5^+$ were made to the 6.6-second and ground states, respectively, taking $\Delta J \geq 5$ from the absence of the gamma transition and $\Delta J \leq 5$ from the shell model. The hypothetical 5^+ ground state was estimated to have a half life of 10^8 years. Further indication appeared in the observation[6] of neutrons unaccompanied by positrons from Mg(p, n)Al for 5.3 Mev > E_p > 3.5 Mev, below threshold for $Mg^{24}(p, n)Al^{24}$ or $Mg^{25}(p, n)Al^{25}$. It will be seen later, however, that these data were spurious.

Cogent evidence for the existence of an isomeric state came from the reaction $Al^{27}(\gamma, n)Al^{26}$, in which the neutron yield is three times the positron yield[7, 8, 9] at a maximum betatron energy of 19 Mev, well above the measured neutron threshold[8] at 13.4 $\pm$ 0.2 Mev.

Unusual theoretical interest attached to the positron decay of Al^{26} as a probable example of a $0 \rightarrow 0$ ($\Delta T = 0$, no) transition. Such transitions are forbidden by the Gamow-Teller selection rules and allowed only by the Fermi interaction. (For a comprehensive discussion of beta decay theory and experiment, see the compendium edited by K. Siegbahn.[10]) The first accurate and definitely established case of this type, the O^{14} - N^{14} beta decay,[11, 12] constituted strong evidence for the existence of the Fermi interaction, about which there had been some question. It has been shown,[13] on the assumption of charge independence of nuclear forces, that the nuclear matrix element for these transitions is

$$\left| \int 1 \right|^2 = T(T + 1) - T_{Z_1} T_{Z_2} ,$$

where T and T_Z are the isotopic spin quantum numbers,[14] this result

being independent of nuclear models. For beta transitions between the lowest T = 1 states of nuclei with mass number A = 4n + 2 (integral n), one has $\left|\int 1\right|^2 = 2$, and with this the value of the Fermi coupling constant, g_F, can be calculated directly from the experimental ft-values. The constancy of g_F determined for many transitions of this kind would be a measure of the validity of the charge independence hypothesis. Kofoed-Hansen has tabulated[15] the (4n + 2)-nuclei for $3 \leq n \leq 14$, giving the expected E_β(max) for the T = 1 transitions calculated from the Coulomb energy difference and the expected half-lives from E_β(max) and the constant ft-value (estimated to be about 2650 seconds). Three of these decays, O^{14}, Al^{26}, and Cl^{34}, are now known to fair precision, and will be discussed later with the results from the present work.

The existence of apparently systematic trends in the odd-odd nuclei has been pointed out by Kofoed-Hansen[15] and by Stahelin,[4,16] notably the decrease with Z of excitation in $T_Z = 0$ nuclei of the lowest T = 1 states which indeed become the ground states in Cl^{34} and K^{38}, and the regular increase with Z of the spins of the lowest T = 0 states within the $1p_{3/2}$ or $1d_{5/2}$-shell. Extrapolation of the spin trend up to Na^{24} leads to spin 5 for Al^{26}, as noted by[17] King and Peaslee.

The $Mg^{25}(p,\gamma)Al^{26}$ reaction was known to have a positive Q-value of 6 or 7 Mev and the positions of numerous resonances were known[1] for production of positron activity. (Some uncertainties of isotopic assignment in early work have been resolved by recent[18,19,20] work with separated isotopes.) A promising attack seemed to be a search by scintillation spectroscopy for resonances at which a direct gamma ray transition to the ground state could be found, or at which the cascade

schemes could be established. A similar plan, as it happened, was being pursued by the Utrecht group, and a preprint of their early report[21] was kindly made available by Dr. S. A. Moszkowski. In it, a resonance at 436-kev bombarding energy, formerly thought to be due to a level in Al^{27} because of the low yield of positrons relative to the yield of gamma rays, was shown to belong to Al^{26}. This result, with the neutron-positron yield ratio, constitutes strong support for the isomeric-state contention. Their work indicated a state in Al^{26} at 0.46 ± 0.08 Mev, on the basis of high energy gamma ray differences, and they proposed it as the 6.6-second, T = 1 state. That this, however, was probably an erroneous assignment was evidenced by the results of Browne's study of the alpha groups from $Si^{28}(d, \alpha)Al^{26}$, published at about the same time. Six levels in Al^{26}, at 0, 0.418, 1.052, 1.750, 1.846, and 2.064 Mev, were assigned from this reaction, but conservation of isotopic spin here inhibits the formation of T = 1 states. The reasonable identification of the 0.46 ± 0.08-Mev state with Browne's 0.418-Mev state suggests the necessity of further search for the 6.6-second state. The later Utrecht results[23] were not available during the present research, and comparisons will be postponed to the final discussions.

B. METHODS AND APPARATUS

For the gamma ray work to be described, thin targets of metallic magnesium of 0.010-inch copper disks were prepared from magnesium oxide (MgO) powder by an evaporation-reduction technique[24] as follows. About 10 to 15 milligrams of MgO were spread over a 1 x 2 cm

area of 0.002-inch tantalum sheet, and the tantalum was heated with electric current in an evacuated system. After outgassing at red heat, an inverted beaker containing target blanks was swung over the tantalum, and the current increased until, at white heat, the inside of the beaker became "half-silvered" at about the target blank distance, the Mg metal coming off by virtue of the reduction of the MgO by the tantalum. Targets prepared in this way were approximately 10 kev thick for 1-Mev protons and withstood currents of one microampere with no observable attrition. Most of the MgO remained unreduced on the tantalum and could be salvaged directly for re-use. The deposit in the beaker was washed off with HCl, precipitated as $Mg(OH)_2$ with KOH, and separated from the liquor by centrifuging. Such frugality was of course only necessary when isotopically-enriched MgO was used. Table I shows the isotopic composition of the electromagnetically enriched magnesium obtained (as MgO) on loan from Oak Ridge and of natural magnesium. Targets referred to later (as Mg^{25}, for example) should be construed to have the isotopic content tabulated here.

TABLE I

Enhanced Isotope	Mg^{24}	Mg^{25}	Mg^{26}	Natural
% Mg^{24} content	99.50	5.87	5.76	78.60
% Mg^{25} "	0.34	92.33	1.08	10.11
% Mg^{26} "	0.16	1.80	96.16	11.29

A satisfactory target for the beta spectrum work with the magnetic-lens spectrometer was made by pressing between the polished surfaces of a steel punch and block, a few milligrams of MgO, spread in a quarter-inch diameter circle on a slightly larger piece of 1-mil aluminum sheet. The resulting disk, with the thin aluminum retained for support, was sandwiched between pieces of 10-mil tantalum with 3/16-inch matching holes. The MgO thickness was 8 mg/cm^2 as determined by weighing with a chemical balance.

Gamma ray detection was accomplished for the most part by means of sodium iodide scintillation spectrometers, which in the past several years have become so familiar a part of laboratory equipment that the general description of the principles involved may safely be left to the literature[10, 25] on the subject. Two crystals were used in this work, one of them (the "small crystal") a right circular cylinder 1.5 inches in diameter by 1.5 inches long, having been described elsewhere[26] in regard to response to gamma rays of various energies. The other (the "large crystal") was a right circular cylinder 4 inches in diameter by 4 inches long, canned in an aluminum housing by the manufacturer, the Harshaw Chemical Company. Its characteristics are discussed in the Appendix. However, since the work reported here was done, the crystal has been recanned by the manufacturer in a new style housing and therefore the bias curves shown in the Appendix for various gamma ray energies are not exactly applicable, due to improved resolution with the new mount. During the course of this work, the energy resolution of the system for gamma rays using the large crystal, was about 11 percent at 1 Mev, while using the small crystal,

it was about 7.5 percent at 1 Mev. The latter was used where accurate energy determination was desired, but the large crystal was very useful for its higher efficiency and for the enhancement of the total absorption peak ("photopeak") of the spectra. Because of the triple-peak structure of gamma ray spectra for $E_\gamma \gtrsim 1.5$ Mev, it is sometimes difficult to make unambiguous energy assignments to several gamma rays occurring simultaneously in the higher energy regions, using only the small crystal spectrum. If both large and small crystal spectra of the same source are available, however, the ambiguity of assignment is considerably reduced, if not removed. An example of this sort will be seen later.

Using high viscosity Dow Corning 200 fluid for good optical contact, the crystals were coupled to the electronics through DuMont end-window, flat-faced photomultiplier tubes, the two-inch type 6292 and the five-inch type 6364. The former, because of its flat-face and higher photocathode luminous sensitivity, has generally supplanted the RCA type 5819 in this laboratory. However, according to Turner and Caldwell,[27] with high counting rates the 6292 does, and the 5819 does not, exhibit an increase of gain having characteristic buildup and persistence times of the order of an hour. This effect was not observed at the low counting rates typical of the Al^{26} investigation, but was troublesome during some of the B^{11}(d, n)-work with the DuMont 6364 photomultiplier. Close fitting μ-metal magnetic shields were used with both the 6292 and 6364, and the systems encased in light-tight containers. Houses of 2-inch lead bricks were always built around the detectors as completely as was practical, and beta rays were kept

out of gamma counters with brass absorbers.

The crystals were used either singly for spectrum analysis, or simultaneously in coincidence arrangements to determine cascade schemes. In the former case, pulses from a preamplifier attached to the photomultiplier tube were shaped by delay-line clipping and amplified in a linear amplifier to pulse heights from 10 to 100 volts. The linear amplifier output was fed to a window amplifier (gain 8) and ten-channel pulse height analyzer combination of the Los Alamos type, which has been described[26, 28] elsewhere. Accurate pulse height comparisons between unknowns and standards were made at the photomultiplier output by coupling the output of a calibrated pulser to the collector. In this way non-linearities of the electronics are by-passed except for the photomultiplier and crystal response. Where accuracy was required, spectrum peaks were always determined at two or more overlapping settings of the window in order to check on channel width uniformity and system stability. In this connection it may be well to note that RC-clipping, with RC-times of the order of a microsecond or less, results in very sharply peaked pulses at the output of the window amplifier for high bias settings, and variations in channel width ensue due to differences in high-speed response among the channels. Delay line clipping avoids this difficulty, but imperfect termination introduces a non-monotonic return to the base line which can be troublesome in fast coincidence circuits.

During the course of this work, a duplicate ten-channel discriminator was finished and put in service. It was convenient to use them

together as a twenty-channel combination (usually with five channels overlapping), all channel biases on one being aligned in slave to the other.

For the gamma-gamma coincidence runs, a portion of the spectrum from one crystal was selected with a single-channel differential discriminator and arranged to provide a standard pulse to gate one ten-channel analyzer. The spectrum from the other crystal in coincidence with the selected region from the first was then recorded in the channels. The properties of the single-channel discriminator made it necessary to use the rather long resolving time of 8 microseconds, but this caused no difficulty because of the low counting rates involved. During the runs, the other ten-channel analyzer recorded the ungated spectrum over the same region, and a monitor counter recorded the number of gates from the single-channel discriminator. Integral bias discriminators monitored the gamma ray yields above the bias settings.

Observations of positron intensities from the 6.6-second state were made with the beam off the target by using a 60-cycle beam deflector and counter gating arrangement. Since the proton beam from the Van de Graaff passed between a portion of the unused electrostatic analyzer plates, it was convenient to use them as the deflector plates by applying to them a square pulse of up to 5 kilovolts during part of (say) the positive halves of a 60-cycle voltage, enough to deflect the beam to an intercepting baffle. The counter would then be gated on, with a delay of about 5 percent of a cycle assuring that the counting period did not overlap the period with the beam on the target.

C. RESULTS

Because of the wide spread in reported values of the endpoint energy for the positron decay, a determination of the positron spectrum was made. The 8-mg/cm^2 pressed target of enriched magnesium oxide was placed at one focus of the magnetic lens spectrometer, with the MgO facing the proton beam from the 3 Mev Van de Graaff generator. A 1-microampere beam of 1.75-Mev energy was used with the beam deflection apparatus, with the positron detector recording only while the beam was off the target. Helical baffles in the lens spectrometer prevented the transit of negative electrons from the target to the geiger counter serving as detector near the other focus of the spectrometer. The construction of the spectrometer (for which see the theses of Hornyak[29] and Rasmussen[30]) prevented the placing of a gamma or beta ray detector sufficiently near to the target to record a statistically significant number of counts for monitoring, so current integration was used for this purpose. Since the beam current was quite steady and the integration time was about four minutes, much longer than the Al^{26} half-life, the current monitor was found quite satisfactory.

The resulting momentum spectrum is shown in Figure 1, and the Fermi plot of these data is shown in Figure 2. The latter points up the unfortunate choice of bombarding energy, about 50 kev above the known $C^{12}(p,\gamma)N^{13}$ resonance at 1.698 Mev (Γ = 70 kev). N^{13} decays by 1.20-Mev positron emission with a half-life of 10.1 minutes, and the deviation from linearity in the low energy part of the Fermi plot is attributed to carbon buildup on the target surface. (The corresponding points on the momentum spectrum were not plotted.) Similar plots

of two preliminary runs restricted to the upper energy region gave the same endpoint as Figure 2 to within 15 kev.

In determining the endpoint energy of the positron spectrum, the principal source of error lies in the choice of background to be subtracted. For example, if the extrapolated background is taken to be ten percent more than that shown in Figure 1, the resulting Fermi plot is still linear, but the endpoint is reduced by 10 kev.

The effect of the traversal of the target material by electrons has been investigated by C. Wong[31] in this spectrometer by measuring the 1.7-Mev P^{32} beta decay with and without a 4.7 mg/cm^2 quartz absorber inserted. The entire spectrum was shifted lower in energy by the absorber, and the difference in the endpoints in the two cases was 8 kev. The value for the energy loss, $dE/(\rho dx)$, that one gets from this is 1.7 Mev/g/cm^2, in good agreement with the value 1.8 Mev/g/cm^2 obtainable from the Feather relation

$$R(g/cm^2) = 0.542E - 0.133, \qquad 0.8 < E < 3 \text{ Mev},$$

for the range of electrons in aluminum as given by[32] Glendenin. Using the former value one gets 25 kev as the correction to be applied in the present case for 8 mg/cm^2 of MgO on 0.001-inch aluminum.

Taking the Fermi plot intersection with the abscissa at 3.190 Mev, one gets 3.21 ± 0.03 Mev for the maximum positron energy. The energy scale was calibrated against the thorium X-line value[33, 34] of 9987 gauss-centimeters, by which the spectrometer constant was found to be 156.88 gauss-centimeters per millivolt. The value for $E_\beta(\max)$ thus obtained agrees with the value calculated from the Coulomb energy

$\frac{6}{5}\frac{e^2}{R}(Z-1) - (M_H - M_n - 2m_o)c^2$, if R is taken to be $1.40A^{\frac{1}{3}} \times 10^{-13}$ cm.

From the difference between $E_\beta(max) + 2m_o c^2$ and the Mg^{26}-Al^{26} Q-value of -4.001 ± 0.028 Mev calculated from nuclear reaction data (see Table II), the excitation energy of the 6.6-second state in Al^{26} is found to be 0.23 ± 0.04 Mev. This confirms Browne's suggestion that none of the states he observed through the $Si^{28}(d,\alpha)Al^{26}$ reaction was likely to be the positron-emitting state, which is now seen to be the first excited state.

TABLE II

Q-values used to calculate the Al^{26}-Mg^{26} mass difference

Reaction	Q-value	Reference
$Mg^{25}(d, p)Mg^{26}$	8.880 ± 0.010	33
$Mg^{24}(d, p)Mg^{25}$	5.097 ± 0.007	35
$Al^{27}(p, \alpha)Mg^{24}$	1.594 ± 0.002	36
$Si^{29}(d, \alpha)Al^{27}$	5.994 ± 0.011	35
$Si^{28}(n, \gamma)Si^{29}$	8.468 ± 0.008	37
$Si^{28}(d, \alpha)Al^{26}$	1.416 ± 0.008	22
Mg^{26}-Al^{26}	-4.001 ± 0.028	

The beam deflection arrangement just described was used in conjunction with two Geiger counters, after a suggestion by Professor T. Lauritsen, to determine the relative yields of positrons and gamma rays as a function of energy, shown in Figure 3. One counter was surrounded with a cylinder of brass having 1/8-inch walls, which to a fair approximation makes a gamma counter with an efficiency[38] proportional to gamma ray energy. Such a counter then gives a measure of the capture cross section regardless of the cascade scheme followed in the decay of the compound state. The linearity was probably less than the best attainable for two reasons. First, the annihilation radiation was not part of the cascade scheme and would add gamma counts favoring positron-yielding resonances. The low efficiency for low energy gammas keeps this effect small. Second, the wall thickness used was just sufficient to stop 4-Mev electrons, and there was therefore a small decrease in response to those captures giving nearly full energy gammas.

The beta counter was of the end-window type (1.4 mg/cm^2 mica), and the target was housed in a thin-walled (26 mils) aluminum tube such that positrons having initial energies greater than about 500 kev would reach the counter. The beta scaler was gated on only when the beam was off the target, verified by the near absence of counts with a 1/8-inch brass plate interposed, and by the five-fold increase in counting rate with reversal of gate phase. The gamma counter was not gated.

The wide variation of the ratio of the two curves in Figure 3 confirms the observation of Kluyver et al. that a varying fraction of the captures must terminate in a state having a half-life much longer than

7 seconds. For example, at 958-kev proton energy, nearly all of the captures go to this state, which, in view of the beta decay and $Si^{28}(d, \alpha)$ results showing a state below the 6.6-second state, should be the ground state.

Shown in Figure 4 are excitation curves, taken with the scintillation counters, overlapping and extending the energy region of Figure 3. The bottom curve gives the yield of annihilation radiation in the small crystal, the 511-kev peak of the pulse height spectrum being selected with a single-channel discriminator. The upper two curves give the yields of the indicated higher energy gamma rays in the large crystal. The relatively low yield of annihilation radiation at 958 kev is also prominent here. The resonance at 873 kev present in both Figures 3 and 4 is attributed to fluorine contamination from an unknown source; fluorine was also present on the back of the target.

Except for the new resonances at 958-kev and 1185-kev, and the doublet-like structures around 990-, 1140-, and 1200-kev bombarding energy, the resonances found here are in agreement with those reported from other laboratories. The resonances assigned to $Mg^{25}(p, \gamma)$ by various observers are collected in tabular form in Table III. The estimated higher-energy members of the two doublets unresolved in this work are enclosed in parentheses. The resonance energies were calibrated to within 7 kev by comparison with the well-known resonances in F^{19} + p at 873.5-, 935.3-, 1346-, and 1372-kev bombarding energy.

The gamma ray spectra at a number of these resonances were examined with the scintillation counters, and the resonances at 721 and 958 kev were selected for careful gamma ray energy measurements and

TABLE III

Resonances in $Mg^{25}(p, \gamma)$ from Various Sources

Reference No.	39	20	23	18	this work	
Percent Mg^{25} in target	10 %	"separated"	91 %	85 %	92 %	
Detected radiation	γ	γ	γ	β	γ	Al^{26*}
E_p (kev)	314.8 ± 0.5	316.7 ± 0.7	321 ± 15			6.621
	389.4 ∓ 0.5	391.5 ∓ 0.5	395	388 ± 10 - 15		6.693
	436.5 ∓ 0.4	436.5 ∓ 0.4	441 (no β^+)			6.737
	484.0 ∓ 1.0	495.6 ∓ 0.6	501	494		6.793
		513.4 ∓ 0.7	518	510		6.810
		530.4 ∓ 0.7				6.827
			580	563		6.86
			607	588		6.89
			667	650		6.95
			688	683	687 ± 7	6.98
				722	721	7.01
				777	778	7.06
				812	817	7.10
				880	887	7.17
				928	933	7.21
					958 (no β^+)	7.24
				986	990	7.27
					(995)	
				1043	1046	7.32
				1081	1086	7.36
				1098	1105	7.38
				1132	1140	7.41
					(1150)	
					1185 ($pp'\gamma$)	7.46
				1197	1199	7.47
					1208	7.48

for coincidence determinations. The choice of the unique 958-kev resonance was made for the obvious reason that its gamma ray decay did not produce the 6.6-second positron-emitting state, and proper summing of these gamma rays would then presumably locate the long-lived ground state. The 721-kev resonance was more or less arbitrarily picked on the basis of its somewhat lower yield, relative to annihilation radiation, of the low energy gamma rays found at 958 kev.

The pulse height spectra taken at these two resonances are displayed in Figures 5 through 10 and the gamma ray energy assignments made from these and other curves taken at different amplifier gains are collected in Table IV. Calibration sources used included: Na^{22}(0.511 and 1.277 Mev); Cs^{137}(0.661 Mev); Th-C'' (2.615 Mev); B^{11} + p (4.43 Mev); and F^{19} + p (6.13 Mev).

TABLE IV

Gamma Ray Energies and Intensities from $Mg^{25}(p, \gamma)Al^{26}$

E_p = 958 kev		E_p = 721 kev	
E_γ (Mev)	Yield (10^{-11} $\frac{\gamma}{p}$)	E_γ (Mev)	Yield (10^{-11} $\frac{\gamma}{p}$)
0.416 ± 0.004	18	0.416	9.1
0.511	2	0.511	10
1.67 ± 0.02	17	0.833 ± 0.006	7.0
2.08	5	1.022 ± 0.006	4.0
(3.0)		1.44 ± 0.03	
5.23 ± 0.05	24	2.46 ± 0.03	2.1
		3.55 ± 0.04	
		5.00 ± 0.05	

Probable energy assignments of the weak gamma rays in the 3- to 4-Mev regions of Figures 6, 9, and 10 are enclosed in parentheses in Table IV because of some uncertainty in the location of the full energy peak. For example, the peak at 3.0 Mev in Figure 9 could conceivably be the "pair-plus-one" peak ($E_\gamma - m_o c^2$) with the "pair" peak ($E_\gamma - 2m_o c^2$) obscured by the 2.5-Mev "photopeak" (full energy, E_γ), or it could be the pair peak. That the peak at 2.5 Mev is indeed a photopeak is clear from its relative enhancement in the large crystal spectrum of Figure 10. The other peaks are then taken to be part of the spectrum of a 3.55-Mev gamma ray, but confusion by the presence of still other gamma rays in this region is possible. The presence of gamma rays with 5.5 Mev $< E_\gamma \leq Q$ can also be seen in Figures 6 and 10, but these have not been resolved.

In addition, because of the crucial role they play in locating the 6.6-second state (as will be seen later), the 0.833- and 1.022- Mev gamma rays were measured by comparison with two similar gamma rays from $Mg^{26}(p,\gamma)Al^{27}$, as shown in Figure 11. In this case the overlapping channels are explicitly plotted, rather than being averaged as usual, to illustrate the scatter involved. The 1046-kev resonance of $Mg^{25}(p,\gamma)$ was used chiefly because of its convenient proximity to the 1050-kev resonance in $Mg^{26}(p,\gamma)$. The energies of the gamma rays from $Mg^{26}(p,\gamma)$ were taken to be 0.843 ± 0.002 Mev and 1.015 ± 0.004 Mev, the former from the electrostatic analyzer measurement of $Al^{27}(p,p')$ by Donahue, Jones, McEllistrem, and Richards[36], the latter from the weighted average of three measurements: 1.013 ± 0.006 by $Al^{27}(p,p')$ in magnetic spectrometer[40], 1.015 ± 0.007 by external conversion in a lens spectrometer[41] of

Mg^{27} - decay gamma rays, and 1.017 ± 0.010 by scintillation spectrometry[42] of $Al^{27}(n, \gamma n')$. The cross-hatching of the arrows indicating peak positions represents the uncertainty allowable for the assigned errors for these gamma rays. Cs^{137} and Na^{22} standard sources checked before and after the two runs determined the photomultiplier drift to be about 0.25 percent (gain increase).

The yields shown in Table IV are the 10-kev-target yields, with a probable error of 20 %, assuming isotropy. Since the resonance widths were all less than the target thickness, these yields are essentially the integrated resonance yields.

The 0.833- and 1.022-Mev gamma rays have an intensity ratio of 9:5, determined from estimated photopeak areas of Figure 11 and corrected by a photopeak efficiency[26] varying as $E^{-1.2}$ for the small crystal. The yields for the former are estimated, from Figure 11 and the geometry involved, as 11×10^{-11} γ/p at the 1046-kev resonance, and, by direct comparison with this, 7×10^{-11} γ/p at the 721-kev resonance. These gamma rays were also observed at the 933-, 990-, and 1086-kev resonances.

At the 958-kev resonance the 0.416-Mev gamma ray yield was 18×10^{-11} γ/p. This gamma ray was also present, in varying ratio to the annihilation radiation, at bombarding energies of 687, 990, 1046, and 1086 kev. It was not present at the 933-kev resonance with more than five percent of the intensity of the annihilation radiation.

The 1185-kev resonance reveals only a 0.588 ± 0.005-Mev gamma ray with a yield of 48×10^{-11} γ/p, other gamma rays from 0.4 to 1.3 Mev having less than about one percent of its intensity; it is therefore

attributed to $Mg^{25}(p, p')Mg^{25*}$ terminating in the known first excited state of Mg^{25}. Since the gamma ray was observed in the forward direction, a 1-kev Doppler correction was subtracted. The state has also been observed[1] via the reactions $Mg^{24}(d, p)Mg^{25}$ and $Al^{27}(d,\alpha)Mg^{25}$, leading to energy assignment of 0.582 ± 0.006 Mev and 0.584 ± 0.006 Mev, respectively.

In order to reduce the ambiguities in the determination of cascade schemes, certain pairs of gamma rays were checked for coincidence, using the system described earlier. The two sodium iodide crystals were placed as close as possible to the target, with shielding arranged to reduce the probability of a gamma ray Compton-scattered from one crystal being detected in the other. Figure 12 shows the results of such a check for the 0.833- and 1.022-Mev gamma rays at the 721-kev resonance. The ordinate scale at the right applies to the self-gated spectrum (dashed curve), the scale at the left to the coincidence spectra. With the single-channel discriminator set to give a gating pulse from pulses originating in the large crystal and having pulse heights corresponding within ten percent to the 1.022-Mev gamma ray, the data plotted as open circles were recorded by the coincidence-gated ten-channel discriminator. The curve strongly suggests that the two gamma rays are in coincidence. As a check, another run was made with the 0.833-Mev gamma ray in the center of the gating window, resulting in the solid circles. The coincidence spectrum is as expected, with the 1.022-Mev gamma ray having about the correct magnitude relative to the previous curve. The presence of the 0.833-Mev photopeak superimposed on the Compton plateau of the 1.022-Mev gamma ray may at first sight seem irregular, but it is

readily accounted for by real coincidences with Compton events of the accepted pulse height from the large crystal due to the 1.022-Mev gamma ray (and higher energy gammas also, to a smaller extent). Real coincidences with the Compton pulses from other gamma rays are the chief source of background counts, the random coincidence rate being less than one percent of the recorded rate in all cases. The random rate was usually computed from the known resolving time, with an occasional check by means of electronically delaying the gating pulse by 30 microseconds. A final verification of the proper functioning of the apparatus and of the above interpretation was made by repeating the measurement with a Mg^{26} target of the same (10 kev) thickness at the 960-kev resonance of $Mg^{26}(p,\gamma)Al^{27}$, which yields two non-coincident gamma rays in the same region. The data are displayed in Figure 13. Since this reaction has a Q-value of 8 Mev, similar to that of $Mg^{25}(p,\gamma)Al^{26}$ (Q = 6.3 Mev), and has about the same capture cross section, the shape and magnitude of the Mg^{26} coincidence spectrum may be taken as a fair representation of the extraneous part of the analogous curve in Figure 12.

At the 933-kev resonance, results nearly identical to those shown in Figure 12 were also obtained. A somewhat smaller yield, $4.4 \times 10^{-11} \frac{\gamma}{p}$ for the 0.833-Mev gamma ray, obtained there.

If all gamma rays with energy greater than 0.9 Mev were in coincidence with the 0.833-Mev gamma ray of Figure 12, the absolute efficiency of the scintillation counter, in the geometry used, for the counts in the photopeak, is exactly the number of counts in the coincidence-gated photopeak (open circles) divided by the number of gates.

Neither the gamma ray interaction cross sections in sodium iodide, nor the source-crystal geometry need be known. Since the number of photopeak counts per microcoulomb in the ungated spectrum is known for the same geometry, the yield can be obtained directly from Figure 12. The yield thus obtained for the 0.833-Mev gamma ray is $7.0 \times 10^{-11} \frac{\gamma}{p}$, in agreement with that calculated from the geometry. This supports the contention that most of the plateau (due to Comptons from higher energy gamma rays) under the 1.022-Mev gamma ray is also in coincidence with the 0.833-Mev gamma ray. As might be expected from the greater intensity of the 0.833-Mev gamma ray, a similar treatment of the other curve of Figure 12 gives a yield for the 1.022-Mev gamma ray about 30 ^{o}/o higher than the value taken from the ungated intensity ratio of 7:4. This excess is consistent with the non-coincident fraction of the gating region around the lower energy photopeak, as can be fairly well estimated from the intensity ratio.

In the same manner, the coincidence of the 0.833- and 5.0-Mev gamma rays was demonstrated, as shown in Figure 14. In this case, uncertainty in the fraction of the self-gated spectrum to be associated with the coincidence spectrum permits only a rough determination of yield. However, if this fraction be taken to be one-half, the resulting value is $6 \times 10^{-11} \frac{\gamma}{p}$. This should also be reduced about 30 ^{o}/o to allow for excess gates, as in the preceding case, if the 5.0-Mev gamma ray is in one-to-one cascade with the 1.022-Mev gamma ray. That this is the situation will be indicated later.

At the 958-kev resonance, the roles of the crystals were reversed,

but the arrangement was otherwise the same. As can be seen from Figures 15 and 16, the 0.416-Mev gamma ray is in coincidence with the 1.67- and 5.23-Mev gamma rays, but not with the 2.08-Mev gamma ray. From Figure 16, the yield of the 5.23-Mev gamma ray is $24 \times 10^{-11} \frac{\gamma}{p}$.

D. DISCUSSION

The problem of fitting the gamma rays into the proper cascade schemes was made considerably simpler by Browne's results from the $Si^{28}(d, \alpha)Al^{26}$ reaction, which are included in the level diagram of Figure 17. In addition to those levels, the beta decay end-point established, as has been seen, a level at 0.23 ± 0.04 Mev.

The absence of positrons at the 958-kev resonance, and the coincidence of the 0.416-, 1.67-, and 5.23-Mev gamma rays, are consistent with the cascade indicated, terminating in the ground state. The 2.08-Mev gamma ray fits well as a cross-over, as suggested by its energy, and the cascade sum puts the resonance level at 7.31 ± 0.05 Mev, consistent with the value 7.24 ± 0.02 Mev obtained from Q-values and the proton resonance energy.

The triply-coincident cascade present at the 721-kev resonance presumably must terminate in the 6.6-second state. Of the three gamma rays, only the 0.833-Mev gamma ray has the proper energy to combine with a known level (1.052 Mev) to produce a state identifiable with the known positron-emitting state, which is thus located at 0.219 ± 0.013 Mev. (The error includes the 8-kev errors assigned by Browne to the energies of the alpha groups.) Assuming that the higher energy member of the remaining two in the cascade proceeds from the resonance

level, a level at 2.074 ± 0.013 Mev is indicated. Either this level or the one at 2.08 Mev implied by the cascade from the 7.24-Mev level could reasonably be identified with Browne's 2.064-Mev level; the reasons for the choice of the latter will be given below. Other cascades must also proceed from the 7.01-Mev level to account for the presence of the 0.416-Mev gamma ray and for the unequal intensities of the 0.833- and 1.022-Mev gamma rays. The latter fact may be combined with the presence of gamma rays of energy 2.46 and 1.44 Mev to suggest a new level at 3.51 Mev. This assignment would also account for the 3.55-Mev gamma ray tentatively assigned to this resonance, 3.5 Mev being the transition energy from the resonance level as well.

On the basis of the shell model, Al^{26} has an odd neutron and proton in $d_{5/2}$ states outside a closed shell. If the low-lying states are assumed to be formed from these by j-j coupling, it follows that states with J = 0, 2, and 4 have $T \geq 1$ and states with J = 1, 3, and 5 have T = 0. This can be seen from the properties of the Clebsch-Gordan coefficients for the combining of two angular moments, j and j', to form a state of angular momentum J:

$$C_{jj'}(J, M; m, m') = (-1)^{J-j-j'} C_{j'j}(J, M; m', m).$$

Here M is the eigenvalue of J_z, etc. Only states of even J have the necessary antisymmetry to have T = 1. Because of its superallowed beta decay and the agreement with the expected location of the analogue of the Mg^{26} ground state, the state at 0.219 Mev is taken to have $J = 0^+$ and T = 1. Since the first known excited state in Mg^{26} lies at

1.83 Mev, presumably in Al^{26} the next T = 1 state lies near 0.22 + 1.83 = 2.05 Mev, and therefore only spins 1^+, 3^+, and 5^+ (assuming even parity) need be considered for the Al^{26} states at 0, 0.416, and 1.052 Mev.

The ground state cannot have $J = 1^+$, or it would decay by allowed positron emission with maximum energy 2.99 Mev, which is contrary to the results at the 958-kev resonance. If it were $J = 3^+$, an allowed transition to the 1.83-Mev state of Mg^{26} would result, taking that state to be either of the remaining T = 1 states indicated above ($J = 2^+$ or 4^+). This would of course also be the case if such a state were to exist at lower excitation in Mg^{26}. Reasonable values for log ft then suggest a half-life of the order of several minutes to several hours, for example, three hours if log ft = 5. This possibility was disproven experimentally by the absence of 1.83-Mev gamma radiation from a thick target of $Mg^{25}O$ which had been bombarded for three hours in a 3/4-microampere beam of 1.5-Mev protons. The spin of the ground state is therefore taken to be $J = 5^+$.

The state of 0.416 Mev is assigned $J = 3^+$, rather than 1^+, since the gamma radiation from it is prompt ($\tau < 10$ μ sec). A $1^+ - 5^+$ transition would have an expected half-life of the order of a few seconds according to the estimate[43] of Blatt and Weisskopf. The remaining $J = 1^+$ is then rather uncertainly assigned to the 1.052-Mev state, consistent with the decay to the 0.219-Mev level.

As mentioned above, the analogue of the 1.83-Mev level of Mg^{26} is expected to lie near 2.05 Mev in Al^{26}, and one might associate either the 2.064- or the 2.074-Mev level with it. However, since the 2.064-Mev state was found from the $Si^{28}(d,\alpha)$ reaction, it should have

T = 0. Furthermore, of the two states it seems most reasonable to assign $J = 2^+$ to the state which does not decay to the $J = 5^+$ - ground state, leaving the other state unassigned except that it should have T = 0 and $J \geq 3$.

These results and conclusions are for the most part in good agreement with those of Kluyver, Van der Leun, and Endt, who investigated the gamma ray spectra at the resonances listed in Table III[23]. Disagreement slightly in excess of the errors exists in the critical measurement establishing the location of the 6.6-second state: they report a gamma ray energy of 0.820 ± 0.004 Mev and place the level at 0.235 ± 0.009 Mev.

A recent accurate determination[2] of the $Mg^{26}(p, n)Al^{26*}$ threshold has been made, from which a beta disintegration energy of 3.202 ± 0.010 can be calculated. (Results from the present work were used to decide that the threshold applies to the first excited state and not to the ground state.) Using this value with 0.219 ± 0.013 for the excitation of the decaying state, the value 4.006 ± 0.016 Mev is found for the $Al^{26} - Mg^{26}$ mass difference.

According to the theory of beta decay, the total decay rate of a beta emitter is given by

$$\lambda(Z, \omega_o) = \frac{\ln 2}{t} = \frac{m^5 c^4}{2\pi^3 \hbar^7} f(Z, \omega_o) \left[g_s^2 \left| M_s \right|^2 + g_T^2 \left| M_T \right|^2 \right]$$

or

$$g_F^2 \left| M_F \right|^2 + g_{GT}^2 \left| M_{GT} \right|^2 = \frac{1.2301 \times 10^{-94}}{f\, t\ (\text{sec.})} \quad \text{erg}^2\text{-cm}^6 ,$$

TABLE V

ft values of known $0^+ - 0^+$ beta transitions

	$T_{1/2}$(sec.)	$E_\beta{}^o$ (kev)	ft (sec)
$O^{14} - N^{14*}$	72.1 ± 0.4 (12)	1835 ± 8 (12)	3275 ± 75
$Al^{26*} - Mg^{26}$	6.58 ± 0.10 (3, 9)	3202 ± 10 (2)	3120 ± 95
$Cl^{34} - S^{34}$	1.53 ± 0.02 (44)	4500 ± 30 (45)	3135 ± 135

where g_F, M_F and g_{GT}, M_{GT} are the interaction constants and nuclear matrix elements for the Fermi and Gamow-Teller interactions, t is the half-life, and f is given in terms of the total decay energy ω_o (units of mc^2) and the atomic number Z of the product nucleus by:

$$f(Z, \omega_o) = \int_1^{\omega_o} F(Z, \omega)\, \omega\, (\omega^2 - 1)^{1/2} (\omega_o - \omega)^2\, d\omega\,.$$

For $\omega^2 \gtrsim 2$, $F(Z, \omega)$ is slowly varying for the cases of interest here, and may be taken in front of the integral as a suitably chosen constant. Feenberg and Trigg[46] suggest $F\left[Z, \frac{1}{2}(\omega_o + \frac{1}{\omega_o})\right]$ for this value, which may then be found from[47] the NBS tables. The above integration can then be carried out to give

$$f/F = (\tfrac{1}{30}\omega_o{}^4 + \tfrac{3}{20}\omega_o{}^2 - \tfrac{2}{15})\sqrt{\omega_o{}^2 - 1} + \tfrac{\omega_o}{4} \ln(\omega_o + \sqrt{\omega_o{}^2 - 1}).$$

In Table V are tabulated the ft-values thus found for the three cases of $0 \longrightarrow 0$ beta decay for which accurate data (references in parentheses) are available. A direct numerical evaluation of ft for Al^{26}, using the

NBS tables, gave ft = 3088 seconds, one percent lower than the value in Table V.

It has already been noted that for these transitions, $|M_{GT}|^2 = 0$ and $|M_F|^2 = 2$, the latter depending only on the charge independence hypothesis. The constancy of the ft-values attests to the validity of that hypothesis.

From the weighted mean, ft = 3200 $\pm$ 54 seconds, one finds that the Fermi interaction constant is

$$g_F = \pm 1.386 \pm 0.012 \times 10^{-49} \text{ erg-cm}^3 \ .$$

The Gamow-Teller constant may also be evaluated from this result and the ft-value (1240 $\pm$ 240 seconds) for the beta decay of[48] the neutron, for which $|M_F|^2 = 1$ and $|M_{GT}|^2 = 3$: expressed as a ratio, $|g_{GT}/g_F| = 1.18 \pm 0.15$. Here the major source of uncertainty lies in the neutron half-life. As far as experimental uncertainties are concerned, a better value for this ratio can be found by using the ft-value, 1014 $\pm$ 20 seconds, for the[49] beta decay of tritium and making the (improbable) assumption that the matrix elements take on their maximum values, which are the same[50] as for the neutron decay. Then one finds that

$$\left|\frac{g_{GT}}{g_F}\right| = \left[\frac{1}{|M_{GT}|^2}\left(\frac{1.2301 \times 10^{-94}}{g_F^2 \ ft} - |M_F|^2\right)\right]^{\frac{1}{2}} = 1.33 \pm 0.03,$$

where the indicated error is the experimental uncertainty. Accurate values for the matrix elements can only increase this value, hence we may conclude that

$$\left|\frac{g_{GT}}{g_F}\right| \geq 1.33 \pm 0.03 .$$

Using this result and reversing the calculation, an upper limit can be placed on the neutron half-life, as has been pointed out by J. M. Blatt[50], viz., $ft \leq 1014 \pm 20$ seconds, or $t \leq 10.5 \pm 0.2$ minutes.

For the $J = 5^+$ ground state, which should decay by positron emission to the 2^+-state of Mg^{26}, by analogy with the $\Delta J = 3$ (no) transition in Be^{10} one may assume a log ft-value of 13.65 to arrive at an estimate for the half-life of 2×10^5 years. Beta and gamma activity with a half-life estimated at about 10^6 years has in fact been observed[51] by the Carnegie Institute group in aluminum chemically separated from a magnesium target after 400 microampere-hours of 15-Mev deuteron bombardment. Handley and Lyon[52] at Oak Ridge have found "long-lived" Al^{26} via the Al^{27}(p, pn) reaction, their sample having exhibited gamma rays with energies 0.717, 1.82, and 2.91 Mev and with relative intensities 0.01, 1, and 0.004, respectively. The 1.82-Mev gamma ray was in coincidence with positrons whose end point was 1.30 ± 0.15 Mev. The 0.717-Mev gamma ray was attributed to Al^{26}, but was not definitely assigned. The 2.91-Mev gamma ray is presumably the result of electron capture, and its weakness suggests that the 2.97-Mev state of Mg^{26} has $J < 4$. Coincidences between 1.83- and 0.511-Mev gamma rays have also been observed by Ferguson[53] from a sample made by deuteron bombardment of magnesium.

Using an anthracene-crystal scintillation spectrometer at the Cavendish Laboratory, Laubitz[54] has determined the shape of the beta spectrum of the ground state decay. The Al^{26} was made by a 630

microampere-hour bombardment of quartz with 5-Mev deuterons, and measurements were started two months later. His results indicated a second forbidden transition with $\Delta J = \pm 2, 3$ (no) and with endpoint 1.17 ± 0.05 Mev, consistent with the $\Delta J = 3$ (no) expected on the basis of the above assignments.

III. BORON PLUS DEUTERON REACTIONS

A. BACKGROUND

Investigators at several laboratories have reported observation of a 15-Mev gamma ray, presumed to originate from the known level at that energy in C^{12}. (The energy level diagram of C^{12}, taken from the review article[55] of Ajzenberg and Lauritsen, is included here as Figure 18 for ready reference, with some additions to bring it up to date.) The earliest report was that of Cohen, Moyer, Shaw, and Waddell, who observed[56] a gamma ray with 15.2 $\pm$ 0.2 Mev energy, using a 180° pair spectrometer at Berkeley, during bombardment of carbon with protons of 30- to 340-Mev energy, and also during bombardment of thick B^{11} targets with deuterons of 18-, 30-, and 50-Mev energy. It was also sought, but not observed, from proton bombardment of Be, B^{10}, and O^{16}, and from alpha bombardment of beryllium. These facts were taken to indicate that the gamma ray originated from the 15.1-Mev level in C^{12} already found via neutron groups[57] from $B^{11}(d, n)C^{12}$. This level is unstable to alpha-emission to states in Be^8 up to 7.7 Mev, and the presence of the gamma radiation led to the suggestion that the state was the B^{12} ground-state analogue, which should lie at about that energy. To the extent that there occurs no mixing, by means of charge dependent interactions, with states having T = 0, breakup into $Be^8 + \alpha$ (or into 3α) in their low-lying states would then be forbidden, and the radiation thus accounted for. However, some such mixing does occur, presumably in the compound state, in the reaction $N^{14}(d, \alpha)C^{12}$, which has been observed[58] to give a thick $N_6C_3H_6$-target yield of 15-Mev gamma radiation of about 3 °/o of the thick B_4C-

target yield ($\sim 3 \times 10^{-5}$ γ/d) from $B^{11}(d, n)C^{12}$ at the same bombarding energy (10.8 Mev) from the Indiana cyclotron. The Indiana group also found a small yield (~ 6 °/o of the B + d yield) of $Be^{9}(\alpha, n\gamma_{15})C^{12}$ using 21.7-Mev alphas. Some inhibition of formation of the 15.1-Mev state might be expected here, if Be^{9} be regarded as made up of two alphas and a neutron loosely bound, since merely replacing the neutron with the incoming alpha could not form a T = 1 state. The chief objective of the present investigation was to determine the extent of the inhibition of alpha breakup of the 15.1-Mev state of C^{12}, as measured by the relative yields of gamma and alpha radiations from that state.

Several additional data regarding the 15.1-Mev level have been reported since this work was started. A proton group from $B^{10}(He^{3}, p)C^{12}$ proceeding to a level at 15.10 $\pm$ 0.1 Mev has been found by Bigham, Allen, and Almqvist at Liverpool[59]; and Fuller, Hayward, and Svantesson[59] have found a photon scattering maximum from C^{12} irradiated with bremsstrahlung from the NBS betatron, corresponding to a level at 15.0 $\pm$ 0.2 Mev. From the difference in the scattered intensity with graphite absorber placed before and after the scatterer, the latter group determined the level width to be $\lesssim$10 kev (the energy of the C^{12} recoil). From the value of 1627 $\pm$ 4 kev for the $B^{11}(d, n)C^{12*}$ threshold reported[61] by Marion, Bonner, and Cook, and the Q-value[62, 63] of 13.734 $\pm$ 0.005 Mev, the level energy can be determined very accurately (see below). A 10.7-Mev gamma ray has also been found by Waddell[64] in $C^{12}(p, p')$, but it was weak compared to the 15.1-Mev radiation and indicates that cascading through the C^{12} 4.43-Mev state is small.

B. METHODS AND APPARATUS

Deuterons having energies up to 3.25 Mev from the Kellogg Laboratory's 3-Mev Van de Graaff generator were used to bombard various boron targets after electrostatic analysis to one or two tenths percent in energy. The somewhat higher energy than had previously been available was obtained as a result of admitting high pressure air into the two supporting columns formerly used for differential pumping of the ion source. About 5 kilograms of Freon (CCl_2F_2) were added to the insulating air to suppress sparking.

Detection of gamma rays was done with the 4" x 4" NaI crystal exclusively, since the smaller crystals available showed little or no peaking in the 15-Mev gamma ray spectrum. Due to the high yield of lower energy gamma rays and neutrons, it was found necessary to reduce the counting rates considerably below target and machine capacity to avoid pile-up and gain drift. The crystal was also shielded with boron-loaded paraffin to attenuate the neutrons and, to some extent, selectively to attenuate lower energy gamma rays. About three inches of paraffin around the sides and up to nine inches in front were typical.

Charged particles were analyzed with the aid of the 16-inch double-focusing magnetic spectrometer, usually using the maximum available solid angle of 0.0063 steradian and a momentum resolution of 230. Calibrations were made with Th-C alpha groups and by well-known reaction Q-values such as that for the omnipresent $C^{12}(d, p)C^{13}$. Since the principal interest was in alpha particle yields, a thin crystal of CsI just thick enough to stop alphas of about 5 Mev was made by milling a CsI wafer glued to a glass slide. The resulting scintillator, mounted

on a DuMont 6292 photomultiplier tube, gave nine percent resolution for 4 Mev alphas. For deuterons the maximum pulse height was achieved at 1.6 Mev, indicating a thickness of 0.007 inch. This is also the range of 1.4-Mev protons and thus simple integral biasing of scalers was sufficient to discriminate in favor of alphas over 3 Mev, giving an advantage statistically over the usual process of finding the difference in counting rates with and without foils. (Magnetic analysis passes protons and alphas having the same energy, and in a thick CsI crystal the proton pulses are somewhat greater than the alpha pulses.)

Thin boron targets were made by evaporation of natural boron (81 ^{o}/o B^{11}, 19 ^{o}/o B^{10}) from tungsten wire onto 3-mil tantalum backing, a typical target being 5.3 kev thick to 800-kev deuterons. However, some of the thickness was due to oxygen and carbon contamination which, after many hours of bombardment, was estimated to be 2.3 kev and 1 kev, respectively, by comparing the $O^{16}(d, p)O^{17}$ and $C^{12}(d, p)C^{13}$ yields in the 16-inch magnetic spectrometer with published[65] cross sections, interpolated in the latter case. Pursuit of accuracy in these estimates was avoided by directly measuring the cross section of the reaction $B^{11}(d, \alpha)Be^{9}$ from the thick target yield curve, using a pure B^{11} target obtained from Harwell. If N_q is the maximum counting rate per q microcoulombs of bombarding particles, after the initial rise, the cross section may be found from[66]

$$\sigma = \frac{N_q R}{q \Omega_c E_2} \left| \epsilon_1 \frac{\partial E_2}{\partial E_1} + \epsilon_2 \frac{\cos \theta_1}{\cos \theta_2} \right| \text{ millibarns,}$$

where R = spectrometer momentum resolution,

Ω_c = solid angle (in center of mass system) of the spectrometer,

E_1 = bombarding energy in electron volts,

E_2 = energy of outgoing particles in electron volts,

θ_1, θ_2 = incident and outgoing angles, measured from the normal to the target on the bombarded side,

ϵ_1, ϵ_2 = stopping cross sections in 10^{-15} ev-cm^2 for the incident and outgoing particles, obtained by interpolation of the curves[67] of Fuchs and Whaling. Then from the integrated yield from a thin target under the same conditions, the surface density, nt, of the specified nuclei (parallel to the incident beam) is

$$10^{-15}\ \text{nt} = \frac{2R}{q\,\Omega_c\,\sigma} \int \frac{N_q(I)}{I}\, dI \quad \text{cm}^{-2} \ ,$$

where I is the fluxmeter reading, inversely proportional to the magnetic rigidity. Direct measurement of the thickness of a thin Harwell target by measuring the shift of the elastic scattering edge was not considered reliable because of the embedding of the boron resulting from the method of manufacture. A check of the scattering profile of the thick target, however, revealed only a negligible mixing of the copper backing with the boron in the first few hundred micrograms per cm^2. It is presumed that with increasing boron deposition the copper atoms in the surface region become increasingly dilute. Then by comparison of the thick-target step with the thin-target integrated yield, the thin target was found to have a surface density of 36 μg/cm^2 (which disagrees with the nominal value of 20 μg/cm^2 indicated by the Harwell label). Interpolated values for ϵ_1 and ϵ_2 used for boron were: $\epsilon_1 = 4.45$ for

1.70-Mev deuterons and 10.3 for 7.2-Mev alpha particles (appropriate to the 58^{o} spectrometer angle).

C. RESULTS

The high energy gamma ray spectrum resulting from the deuteron bombardment of the 36-$\mu g/cm^2$ B^{11} target is shown in Figure 19 for two bombarding energies. The difference between the yields is then plotted as solid circles and taken to be the net yield of 15-Mev radiation from 50 to 80 volts pulse height. The lowest point of the curve was extrapolated to zero pulse height as a constant Compton plateau, the total area thus formed giving the total yield used to determine the cross section for the reaction. The counter efficiency was found by numerical integration as indicated in the appendix, and a 5 $^{o}/o$ correction applied for the absorption of the paraffin interposed. In calculating the latter, only the pair production cross section in CH_2 was used, since, at this high gamma ray energy, the Compton-scattered gamma rays are nearly all forward and lose little energy, and in the geometry used would largely be intercepted by the crystal.

The $B^{11}(d, n\gamma)C^{12}$ cross section at 2.2 Mev was thus found to be 29 ± 7 millibarns. The radiation was approximately isotropic at 2.5 Mev, with $I(90^{o})/I(0^{o})$ increasing slowly with decreasing energy to a value of 1.15 at 1.7 Mev (just above threshold).

The lower energy tail shown in Figure 19 for 1.59-Mev deuteron energy decreased smoothly in intensity with bombarding energy, at 550 kev the yield above 50 volts pulse height being about one-tenth that at 1.6 Mev. Also shown is the gamma ray spectrum at 796-kev bom-

barding energy obtained with the "thick" Harwell B^{11} target (which was found by alpha yield from $B^{11}(d, \alpha)Be^{9}$ to have a thickness of about 600 $\mu g/cm^2$ although labeled 100 $\mu g/cm^2$). The peak in the spectrum is appropriate to a gamma ray of 12.8 $\pm$ 0.3 Mev, calibrated in terms of the 15.1-Mev peak in the figure. The yield per microcoulomb was independent of the beam intensity, hence random coincidence of lower energy pulses was not involved here. The possibility of real coincidences between the 4.43-Mev gamma ray and its accompanying fast neutron was ruled out on the basis of known or limiting values of cross sections, the geometry involved, and the resolving time of one microsecond allowable for neutron scattering time. That proton contamination of the mass two beam was not the source, through the known 12-Mev gamma ray from $B^{11}(p, \gamma)C^{12}$, was checked by verifying that the yield was non-resonant and small over the deuteron energy range 300 to 356 kev, spanning the known proton resonance at 163 kev. It is therefore concluded that it is a real gamma ray and that it originates from a state in C^{12} at 12.8 Mev, perhaps the known state at 12.76 Mev. The cross section for its production at 1.6 Mev is estimated to be about 4 $^{o}/o$ of that for the 15.1-Mev gamma ray at 2.2 Mev, or about 1.2 millibarns. Waddell has also observed[64] a small yield of 12-Mev gamma radiation from $C^{12}(p, p')$, barely resolved from a much larger yield of the 15-Mev radiation in the pair spectrometer.

Since the 12.8-Mev level in C^{12} is unstable by over 2 Mev to alpha-emission to the 2^{+}-state of Be^{8}, as well as to the 0^{+}-ground state, gamma emission is surprising, and would seem to warrant further study. The reaction $B^{11}(He^{3}, d)C^{12}$ may offer a possible channel,

free of obscuration by the 15-Mev gamma ray and with a threshold at about 2.9 Mev.

The yield of the 15.1-Mev gamma ray from a thin evaporated target, as a function of bombarding energy, is shown in Figure 20 (the curve labeled α-yield will be discussed later). The points were obtained with the ten-channel discriminator set to span the peak of the spectrum at about half maximum, and the sum of the channels plotted. Two resonances, presumably from the formation of the compound states of C^{13} at 20.5 and 21.3 Mev, are evident at 2.180 and 3.080 Mev, respectively. The difference between the actual curve and a smooth interpolation of the larger trend around 2.2 Mev is plotted to emphasize the resonance structure. The level widths are 135 and 190 kev, respectively.

Details of the threshold are shown in Figure 21, exhibiting the $\sqrt{E - E_o}$ shape to be expected for s-wave outgoing neutrons. The threshold is quite sharply defined and was determined to be 1633 $\pm$ 3 kev by comparison with the $Li^7(p, n)$ threshold at 1881.0 $\pm$ 1 kev from a metallic lithium target freshly evaporated in situ. Small corrections for relativistic mass increase and target potential were made. A limit of about 2 kev for the level width is evident from the sharpness of the rise from this 3-kev target; however, a smaller limit will be found below. From the average of this threshold energy and 1627 $\pm$ 4 kev from the work of Marion et al.[61], the excitation of the state in C^{12} is 15.111 $\pm$ 0.006 Mev. It has been pointed out by Professor T. Lauritsen that this accurately known, readily detected threshold provides a convenient calibration point for deuteron accelerators.

In an attempt to detect alpha particles from the decay of the 15.1-Mev state, the charged particle spectrum from the thin evaporated target was investigated with the 16-inch spectrometer, at a deuteron energy of 1.70 Mev and at a laboratory angle of 58^{o}, as is shown in Figure 22. Alpha particles (open circles) were separated from other charged particles (solid circles) at the same momentum by pulse height selection, a typical bias curve being shown in Figure 23. It is sufficient for the moment to note only that the alphas are well separated from the other groups. In Figure 22, the lowest energy shown is at the Rutherford scattering edge, below which pile-up of pulses prevented investigation of the alpha spectrum. The various groups are identified uniquely by labeling them with the final state, for example, the oxygen and carbon contamination is manifested in the three peaks from $O^{16}(d, p)O^{17}$, $O^{16}(d, \alpha)N^{14}$, and $C^{12}(d, p)C^{13}$. The contribution from the B^{10} content of the target was investigated with a separated (96 ^{o}/o B^{10}) evaporated target, and is shown in the upper inset, with ordinates normalized to give the same number of counts in the $B^{10}(d, p)B^{11*}$ (6.76)-peak. The nearly constant counting rate over the entire region is attributed to the three-body breakup $B^{10} + d \rightarrow 3He^{4}$. Final states in Be^{8} from the reaction $B^{10}(d, \alpha)Be^{8*}$ between 9.8- and 14.8-Mev excitation were covered, extending above the range (0 to 11.3 Mev) investigated recently by[68] Holland, Inglis, Malm, and Mooring. The states[69] at excitations of 11.1 and 14.7 Mev reported from the reaction $Li^{7}(d, n)$ are not evidenced here, and have cross sections of less than 2 millibarns per steradian for production by $B^{10}(d, \alpha)Be^{8}$ at the energy and angle shown in Figure 22.

The $B^{11}(d, \alpha)Be^{9}$ cross section having been found, as noted above, the other boron-reaction cross sections giving peaks in Figure 22 were calculated. The O^{16}-contamination was also known by comparison (at E_l = 2.65 Mev) with the $O^{16}(d, p)O^{17}$ cross sections given by Stratton et al.[65], thus permitting determination of cross sections at E_l = 1.70 and $\theta_{LAB} = 58^{\circ}$, as follows:

Reaction	σ cm (mb/st ± 15 %)
$O^{16}(d, p)O^{17}$ (0)	7.0
$O^{16}(d,\alpha)N^{14}$ (0)	3.8
$B^{10}(d, p)B^{11*}$ (6.76)	6.1
$B^{11}(d, \alpha)Be^{9*}$ (3.02)	0.80
$B^{11}(d, \alpha)Be^{9*}$ (2.43)	1.85
$B^{11}(d, \alpha)Be^{9}$ (0)	3.94

The peak indicated as a state at 1.75 Mev in Be^{9} may well be due rather to the three body breakup $B^{11} + d \rightarrow Be^{8} + n + \alpha$, as discussed[70] by Rasmussen, Miller, Sampson, and Wall in connection with inelastic scattering of deuterons from beryllium.

In addition to the well-defined groups and the B^{10} contribution, there remains the broad yield of alpha particles with a maximum in the region labeled "A", attributed to the multi-body reaction $B^{11} + d \rightarrow 3\,\alpha + n$ which gives a maximum alpha energy near "B", and to the break-up of the broad 3-Mev state in Be^{8} which gives alpha energies extending down from about 5 Mev. Alphas from the decay of the 15.1-Mev state in C^{12} to the ground state of Be^{8} would exhibit a peak at B somewhat larger than the adjacent Be^{9*}(2.43)-peak if isotropic and as probable as

the gamma emission. The transition is forbidden if the 15.1-Mev state has $J = 1^+$ as expected. Transition to the Be^8 excited state is not forbidden by angular momentum considerations, however, and should give a broad alpha group centered at A, the width being determined by the[68] width (~1 Mev) of the Be^{8*}. With the 16-inch spectrometer set near A, therefore, the yield of alphas as a function of bombarding energy was determined, the spectrometer being varied simultaneously over a range of 370 kev to avoid the scattering edge. The separated B^{11} thin target, which had negligible oxygen content, was used to obtain the curve incorporated as part of Figure 20. The dashed curve shows the expected additional yield from the state in question if the alpha- and gamma-widths were equal; the results indicate that $\Gamma_\alpha < \frac{1}{2} \Gamma_\gamma$, allowance having been made for the statistical weight favoring alpha-emission.

In Figure 22, the region at "C" in the insert is the expected location, at the higher bombarding energy, of the ground state alpha group from the next T = 1 state of C^{12} at 16.1 Mev, well-known[55] from the reaction $B^{11}(p,\alpha)Be^8$. About 2 °/o of the decays proceed by long-range alphas, and its absence here at 160 kev above threshold indicates a cross section for production of the state of less than 10 millibarns, if the alphas are isotropic.

The remainder of the pulse height spectrum (Figure 23) below the alpha peak consists of the proton peak at 18 volts, and an unidentified peak at 8 volts. The dashed curve was taken at 50 °/o more gain, thus moving the unknown peak to 12 volts and revealing another rise at still lower pulse height. The latter was separately investigated and identified

as recoil C^{13} nuclei from $C^{12}(d, p)C^{13}$, using a thin target of natural carbon. The counts from 30 to 50 volts are presumed to be "ghosts" from multiply scattered deuterons.

Since much of the discussion of the 15.1-Mev state in C^{12} depends upon its identification as the analogue of the B^{12} ground state, a measurement of the branching of the B^{12} beta decay was made. The spins of both the ground state (0^+) and first excited state (2^+) being known, establishment of the ft-values for the two branches could be used to infer the spin and parity of B^{12}. Early work[71] by Hornyak and Lauritsen had accurately fixed the endpoint of the ground state transition as 13.43 ± 0.06 Mev, and found about 5 °/o branching to higher states, which were, however, not specified with any certainty. Similarly, beta-gamma coincidences by Vendryes[72] showed 4 ± 1 °/o higher transitions, but the assignment to the first excited state of C^{12} was not considered to be established.

In this experiment, the B^{12} was made via $B^{11}(d, p)B^{12}$ by bombarding a thick target of natural boron, pressed into a thin aluminum thimble, with 400-kev deuterons from the 3-Mev Van de Graaff, magnetically analyzed. The target was housed in a thin-walled lucite chamber, with beta and gamma detectors placed as shown in Figure 24. The beta rays were detected with a plastic scintillator 1.75 inches in diameter by 11/16 inch thick, mounted in an aluminum can on a DuMont 6292 photomultiplier. The four-inch NaI crystal was used as gamma detector, with 3.6 centimeters of graphite interposed to absorb the beta rays with a minimum of bremsstrahlung production. Because of the tremendous yield of prompt gamma and neutron radiation, the beam

deflection apparatus already described was used here, such that all counting was done with the beam off the target and intercepted by a tantalum sheet above the magnetic analyzer. The 60-cycle deflection rate was well suited to the B^{12} half-life of 23 milliseconds.

A block diagram of the electronics involved is included in Figure 24. The gamma ray spectrum was displayed on the ten-channel analyzer, which was allowed to record pulses only if a beta-gamma coincidence occurred within the resolving time (0.4 μ sec) of the fast coincidence mixer. To correct for differences in crystal rise times and in electronics delays, a suitable length of RG65U delay cable was inserted in the beta-channel, the length being determined by a direct check of gamma-gamma coincidences from Na^{22} annihilation radiation. A plot of counting rate versus delay inserted also gave a direct measure of the resolving time of the system. Random coincidences were counted by inserting a long (1 μ sec) delay in place of the 0.2-μ sec used during the counting of real coincidences.

The beta-channel was biased such that Cs^{137} gamma rays ($h\nu$ = 661 kev) were just excluded, to reduce x-ray background. Thus, considering also the absorption due to the material in the path of the beta rays, it is calculated that electrons originating in the target with energies greater than 1.9 Mev were counted. Since this effective bias cut out a larger fraction of the transitions to the 4.4-Mev state than those to the ground state, a calculated correction factor of 1.066 was applied to the measured gamma/beta ratio. The beta counting rate was reduced to 1 $^{o}/o$ by $\frac{1}{4}$ - inch of brass.

The low bombarding energy and low currents ($\sim$ 0.2 microampere) were selected to minimize machine background and difficulties due to the

high yields, especially the gain drift of the gamma counter. Even so, it was found desirable to season the counter with a half-hour run with the beam on the target, before starting the recorders. The importance of gain stability was increased by the necessity of successive long runs (about one-half hour each) with the ten-channel analyzer spanning overlapping parts of the spectrum.

The results of the best of four runs are shown in Figure 25, where the open circles represent the recorded counts minus the measured randoms, the latter being indicated by the solid circles. The crosses, through which the curve is drawn, are an overlay of the spectrum from $N^{15}(p,\alpha\gamma)C^{12}$, which gives a clean spectrum of the gamma ray from C^{12*}. The fit is seen to be good except at the lower pulse heights, where there appears a subsidiary peak. This is attributed to real beta-gamma coincidences from Al^{28}, which is known[1] to decay by a 2.9-Mev beta transition followed by a 1.8-Mev gamma ray, with a 2.3-minute half-life.

A net total of 13000 coincidence counts is represented by the plotted points plus the Compton tail extrapolated to zero pulse height. From this and other similar runs, it was calculated that (1.3 ± 0.4) percent of B^{12} decays are followed by the 4.4-Mev gamma ray. Various correction factors were applied as follows: + 6.6 %/o for beta counter bias, as mentioned above; + 8 %/o for the absorbers in the path of the gamma rays; -19 %/o for dead time in the number four scalar (the dead time was measured using two radioactive gamma sources singly and together). The total efficiency of the gamma detector was calculated to be 5.8 %/o from the geometry and NaI cross sections. The gamma

absorption by the carbon block was taken to be half that computed from the total gamma ray absorption cross section.

It can also be estimated from the small number of net counts from pulses over 60 volts that (0.00 ± 0.01) percent of transitions are accompanied by a gamma ray having an energy greater than 6 Mev. Furthermore, from the absence, in Figure 25, of a 3.2-Mev gamma ray, it can be said that less than (0.1 ± 0.1) percent of the beta transitions lead to the known 7.67-Mev state in C^{12} followed by gamma decay. This, of course, does not preclude a stronger transition followed by alpha decay to Be^{8}, which is known[73] to occur.

Essentially the same conclusions have been reached by N. Tanner[74], who finds a (1.7 ± 0.4) percent branch to the 4.43-Mev state of C^{12}. He was also able, by gamma-gamma coincidences, to put a limit of (0.04 ± 0.2) percent on the transitions accompanied by a 3.2-Mev gamma ray. (The probability of gamma decay of the 7.67-Mev state of C^{12} is of considerable importance in connection[73] with the stellar production of heavy elements, but will not be discussed here.)

A thin target yield curve for $B^{11}(d, p)B^{12}$ was also found, using the same counters with the 60-cycle beam deflector arrangement, but without the fast coincidence. In this case, the gamma counter was placed at 90°, about six inches from the target, and biased to observe the 15-Mev radiation for use in energy calibration of the magnetic analyzer. The gamma ray yield also allowed an approximate check on the B^{11} content of the target. The beta counter was placed at 0°, four inches from the target, with a 2-Mev bias. The net effect of

absorber plus bias was estimated to be such as to allow electrons from the target to be counted if their initial energy exceeded 3 Mev.

The results are shown in Figure 26. The dashed curve at the bottom shows the counting rate when 1/8-inch brass plus 1/8-inch lead were placed in the path of the beta rays. No indication is to be seen of the resonances in the yield which were apparent in the gamma ray yield from the production of the analogue state in C^{12} via $B^{11}(d,n)C^{12*}$, suggesting the predominance of stripping in the present instance.

Although an accurate value for the absolute cross section was not sought, it can nevertheless be estimated from the data to an accuracy of about 50 percent, and the ordinates of Figure 26 have accordingly been so labeled. Corrections were made for the bias and absorption, for the effect of the 60 cycle chopper on the counting rate, and for the solid angle (1 ^{o}/o of 4π). From the geometry of the system, scattering of electrons into the counter is deemed small. At 1.5-Mev bombarding energy, the value thus found was 380 millibarns, in violent disagreement with the value of 4 millibarns found[75] by Hudspeth and Swann.

D. CONCLUSION

From the 1.3 ^{o}/o branching of the B^{12} beta decay to the 4.4-Mev state of C^{12}, and the known half life and end-points, the ft-value for the weaker transition is found to be log $(ft)_1 = 5.2$, putting it in the allowed (unfavored) class. The ground state transition has log $(ft)_o = 4.17$. Thus the transitions to both the 0^+ ground state and the 2^+ excited state are allowed, fixing the B^{12} ground state uniquely as $J = 1^+$. It has been pointed out[76] that the possibility of $J = 0^+$, which might be

advanced, is forbidden by the isotopic spin selection rule for the ground state transition.

The identification of the 15.1-Mev state in C^{12} as the analogue of the B^{12} ground state thus determines the gamma radiation as magnetic dipole. The radiation width may then be estimated from the single-particle transition probabilities given by Blatt and Weisskopf[43] to be 70 ev, which may be regarded as an upper limit, since the single-particle matrix elements are liberal, in general. Since Γ_a has been shown to be less than $0.5\Gamma_\gamma$, this limit on the radiation width may be considered to be the upper limit on the total width of the state.

Fuller et al.[60] give a mean scattering cross section of 0.7 ± 0.2 mb. for the reaction $C^{12}(\gamma, \gamma'_{15})C^{12}$ for $1.4 \leq E_\gamma \leq 15.8$ Mev, which, as suggested by Dr. Christy, now permits calculation of fairly restrictive limits on Γ_γ and thus on the total width Γ. Assuming a Breit-Wigner form for the cross section, one finds

$$\bar{\sigma}\,\Delta E \equiv \int_{\Delta E} \sigma\, dE \doteq \pi\lambda^2 \int_{-\infty}^{\infty} \frac{\omega \Gamma_\gamma^2\, dE}{(E-E_R)^2 + \left(\frac{\Gamma}{2}\right)^2} = 2\pi^2 \lambda^2 \omega \frac{\Gamma_\gamma^2}{\Gamma}$$

where $\omega = 3/2$ is the statistical factor. Then, since $\Gamma_\gamma < \Gamma < 1.5\Gamma_\gamma$, and within the 30 °/o accuracy to which $\bar{\sigma}\Delta E$ is given, 19 ev $< \Gamma_\gamma <$ 28 ev, and 19 ev $< \Gamma <$ 43 ev.

APPENDIX

Although the subject of scintillation spectroscopy is well-covered by available literature[10], the specific properties of scintillators of various types and sizes are sufficiently different to require individual treatment. In the present case, it is necessary for cross section determinations to know the total efficiency and the pulse height distribution for gamma rays of various energies interacting with a sodium iodide cylinder four inches in length and diameter.

The principal fundamental interactions occurring for gamma ray energies above about 200 kev are photoelectric absorption, Compton scattering, and pair production, which are well-understood theoretically and for which cross sections[77] have been tabulated. Since the occurrence of any single or cascade interaction in the crystal is recorded as one event somewhere in the pulse spectrum, it is sufficient to know the sum of the fundamental cross sections to calculate the total efficiency for any given geometry. The probability of cascade absorption then determines the pulse height distribution characteristic of the crystal size, geometry, and collimation. A detailed discussion of this point may be found in an article by Foote and Koch[78], who also display typical pulse height spectra from a large (5" D x 4" L) NaI (Tl) scintillator.

Shown in Figure 27 is a series of pulse height distributions from the 4 x 4-inch crystal for monoenergetic gamma rays of various energies. The gamma rays of energy less than 3 Mev were collimated along the crystal axis through a 1-1/2-inch diameter hole in 4 inches of lead, while those of greater energy were uncollimated. The curves have all been

normalized to have the same area and to place the photopeak (more properly, the total absorption peak) at 10 on the abscissa. The Compton plateau in each case has been extrapolated smoothly to zero pulse height as indicated by the dashed lines. In the cases $F^{19}(p, \gamma)$ and $C^{13}(p,\gamma)$, the contributions of other gamma rays in the regions near the peaks have been subtracted (the amounts in the two cases were, respectively: $\gamma_{7.1}/\gamma_{6.1} = 0.28$ at $E_p = 873$ kev and $\gamma_{6.5}/\gamma_{9.2} = 0.13$ at $E_p = 1.76$ Mev). Of the total counts the fraction appearing in the photopeak (the "photofraction") is somewhat dependent on the geometry; for example, it drops from 67 °/o for Cs^{137} (0.661 Mev), collimated as above, to 56 °/o for an uncollimated Cs-source.

The results of an illustrative calculation of the total efficiency of the 4-inch crystal are shown in Figure 28, for a source centered two inches from the crystal face, In evaluating the efficiency integral, the absorption in the central frustrum of a cone was taken to be the average of the extremes, while the remainder was found by numerical integration. A fractional change in efficiency of approximately 7 °/o results from a change of 0.1 inch in the source distance for this case. Also shown are the photofractions taken from the curves of Figure 27, the low energy sides of the photopeaks being completed symmetrically with the upper sides.

REFERENCES

1. P. M. Endt and J. C. Kluyver, Revs. Modern Phys. 26, 95 (1954).

2. Kington, Bair, Cohn, and Willard, Phys. Rev. 99, 1393 (1955).

3. Churchill, Jones, and Hunt, Nature 172, 460 (1953).

4. P. Stahelin, Helv. Phys. Acta 26, 691 (1953).

5. D. Maeder and P. Stahelin, Helv. Phys. Acta 28, 193 (1955).

6. P. Stahelin, quoted in (ref. 1).

7. Montalbetti, Katz, and Goldemberg, Phys. Rev. 91, 659 (1953).

8. Haslam, Roberts, and Robb, Can. J. Physics 32, 361 (1954).

9. L. Katz and A. G. W. Cameron, Phys. Rev. 84, 1115 (1951).

10. K. Siegbahn (Ed.), Beta and Gamma-Ray Spectroscopy, North-Holland Publishing Co., Amsterdam, 1955.

11. R. Sherr and J. B. Gerhart, Phys. Rev. 91, 909 (1953).

12. J. B. Gerhart, Phys. Rev. 95, 288 (1954).

13. E. P. Wigner, Phys. Rev. 56, 519 (1939).

14. The isotopic spin formalism is discussed in Blatt and Weisskopf, Theoretical Nuclear Physics, John Wiley and Sons, New York, 1952.

15. O. Kofoed-Hansen, Phys. Rev. 92, 1075L (1953).

16. P. Stahelin, Phys. Rev. 92, 1076L (1953).

17. R. W. King and D. C. Peaslee, Phys. Rev. 90, 1001 (1953).

18. Taylor, Russell, and Cooper, Phys. Rev. 93, 1056 (1954): Mg^{25} + p, β^+-yield versus energy, 350 kev $\leq E_p \leq$ 1200 kev.

19. Russell, Taylor, and Cooper, Phys. Rev. 95, 99 (1954): Mg^{26} + p, γ-yield versus energy, 300 kev $\leq E_p \leq$ 1550 kev.

20. S. E. Hunt and D. A. Hancock, Phys. Rev. 97, 567L (1955): Mg^{25} γ-yield and natural Mg β^+-yield, 200 kev $\leq E_p \leq$ 550 kev.

21. Kluyver, van der Leun, and Endt, Phys. Rev. 94, 1795L (1954).

22. C. P. Browne, Phys. Rev. 95, 860L (1954).

23. Kluyver, van der Leun, and Endt, Physica 20, 1287 (1954).

24. Russell, Taylor and Cooper, Rev. Sci. Instr. 23, 764 (1952).

25. R. D. Evans, The Atomic Nucleus, McGraw-Hill, New York 1955.

26. H. H. Woodbury, Ph. D. Thesis, Calif. Inst. of Tech. (1953).

27. R. L. Caldwell and S. E. Turner, Nucleonics 12, No. 12, 47 (1954).

28. C. W. Johnstone, Nucleonics 11, No. 1, 36 (1953).

29. W. F. Hornyak, Ph. D. Thesis, Calif. Inst. of Tech. (1949).

30. V. K. Rasmussen, Ph. D. Thesis, Calif. Inst. of Tech. (1950).

31. C. Wong. Ph. D. Thesis, Calif. Inst. of Tech. (1953).

32. L. E. Glendenin, Nucleonics 2, No. 1, 12 (1948).

33. G. L. Lindstrom, Phys. Rev. 87, 678 (1952).

34. W. L. Brown, Phys. Rev. 83, 271 (1951).

35. Van Patter, Sperduto, Endt, Buechner, and Enge, Phys. Rev. 85, 142 (1952).

36. Donahue, Jones, McEllistrem, and Richards, Phys. Rev. 89, 824 (1953).

37. B. B. Kinsey and G. A. Bartholomew, Can. J. Physics 31, 537 (1953).

38. Fowler, Lauritsen, and Lauritsen, Revs. Modern Phys. 20, 236 (1948).

39. S. E. Hunt and W. M. Jones, Phys. Rev. 89, 1283 (1953).

40. Browne, Zimmermann, and Buechner, Phys. Rev. 96, 725 (1954).

41. H. Daniel and W. Bothe, Zeit. f. Naturf. 9A, 402 (1954).

42. R. B. Day, Phys. Rev. 89, 908A (1953) and Phys. Rev., to be published.

43. J. M. Blatt and V. F. Weisskopf, Theoretical Nuclear Physics, Wiley and Sons, New York, 1952; p. 627.

44. R. M. Kline and D. J. Zaffarano, Phys. Rev. 96, 1620 (1954).

45. D. Green and J. R. Richardson, Phys. Rev. 101, 776 (1956).

46. E. Feenberg and G. L. Trigg, Revs. Modern Phys. 22, 399 (1950).

47. Tables for the Analysis of Beta Spectra, NBS Applied Math Series, No. 13.

48. J. M. Robson, Phys. Rev. 83, 349 (1951).

49. L. M. Langer and R. J. D. Moffat, Phys. Rev. 88, 689 (1952).

50. J. M. Blatt, Phys. Rev. 89, 83 and 86 (1953).

51. Simanton, Rightmire, Long, and Kohman, Phys. Rev. 96, 1711L (1954).

52. T. H. Handley and W. S. Lyon, Phys. Rev. 99, 755 (1955).

53. J. M. Ferguson, MIT Progress Report, Aug. 31, 1955.

54. M. J. Laubitz, Proc. Phys. Soc. (London) 68A, 1033 (1955).

55. F. Ajzenberg and T. Lauritsen, Rev. Mod. Phys. 27, 77 (1955).

56. Cohen, Moyer, Shaw, and Waddell, Phys. Rev. 96, 714 (1954).

57. V. R. Johnson, Phys. Rev. 86, 302 (1952).

58. Rasmussen, Rees, Sampson, and Wall, Phys. Rev. 96, 812L (1954).

59. Bigham, Allen, and Almqvist, Phys. Rev. 99, 631A (1955).

60. Fuller, Hayward, and Svantesson, Bull. Am. Phys. Soc. 1, 21 (1956).

61. Marion, Bonner, and Cook, Phys. Rev. 100, 847 (1955).

62. D. M. Van Patter and W. Whaling, Rev. Mod. Phys. 26, 402 (1954).

63. J. Mattauch and R. Z. Bieri, Naturf. 9, 303 (1954).

64. C. N. Waddell, private communication.

65. Stratton, Blair, Famularo, and Stuart, Phys. Rev. 98, 629 (1955); Bonner, Eisinger, Kraus, and Marion, Phys. Rev. 101, 209 (1956); G. C. Phillips, Phys. Rev. 80, 164 (1950).

66. Snyder, Rubin, Fowler, and Lauritsen, Rev. Sci. Inst. 21, 852 (1950).

67. R. Fuchs and W. Whaling, Stopping Cross Sections (to be published).

68. Holland, Inglis, Malm, and Mooring, Phys. Rev. 99, 92 (1955).

69. Whitehead, Phys. Rev. 79, 393 (1950).

70. Rasmussen, Miller, Sampson, and Wall, Phys. Rev. 100, 851 (1955).

71. W. F. Hornyak and T. Lauritsen, Phys. Rev. 77, 160 (1950).

72. G. Vendryes, Compt. Rend. 233, 391 (1951).

73. Cook, Mozer, Fowler, and Lauritsen, to be published.

74. N. Tanner, Phil. Mag. 1, 47 (1956).

75. E. L. Hudspeth and C. P. Swann, Phys. Rev. 76, 1150 (1949).

76. A. B. Clegg, private communication.

77. G. R. White, NBS Report No. 1003 (May 1952).

78. R. S. Foote and H. W. Koch, Rev. Sci. Inst. 25, 746 (1954). See also J. W. Motz, Phys. Rev. 100, (1955).

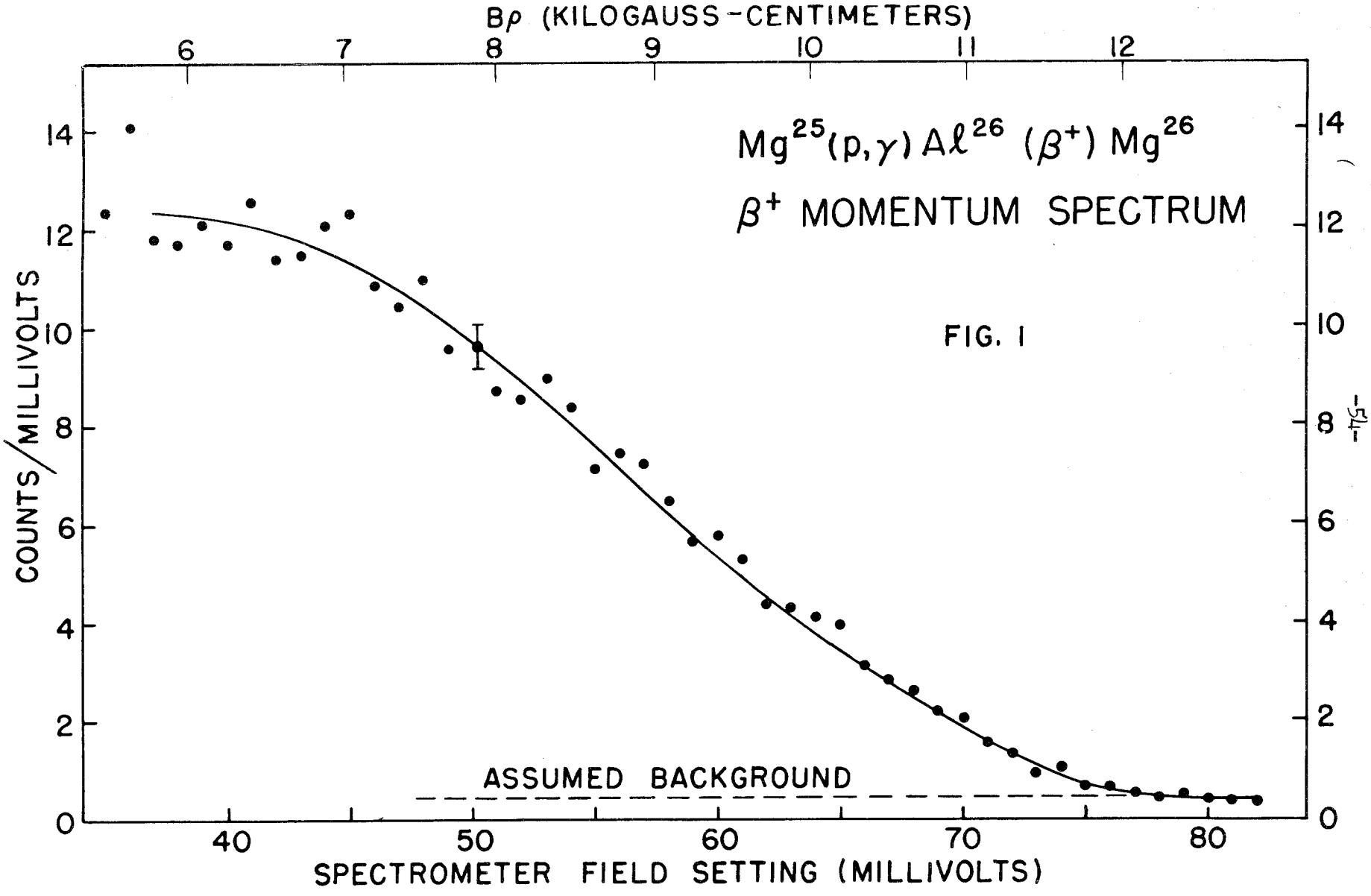
Bρ (KILOGAUSS-CENTIMETERS)
6
7
8
9
10
11
12
$Mg^{25}(p,\gamma)\,Al^{26}\,(\beta^+)\,Mg^{26}$
β^+ MOMENTUM SPECTRUM
FIG. 1
COUNTS/MILLIVOLTS
0
2
4
6
8
10
12
14
ASSUMED BACKGROUND
40
50
60
70
80
SPECTROMETER FIELD SETTING (MILLIVOLTS)

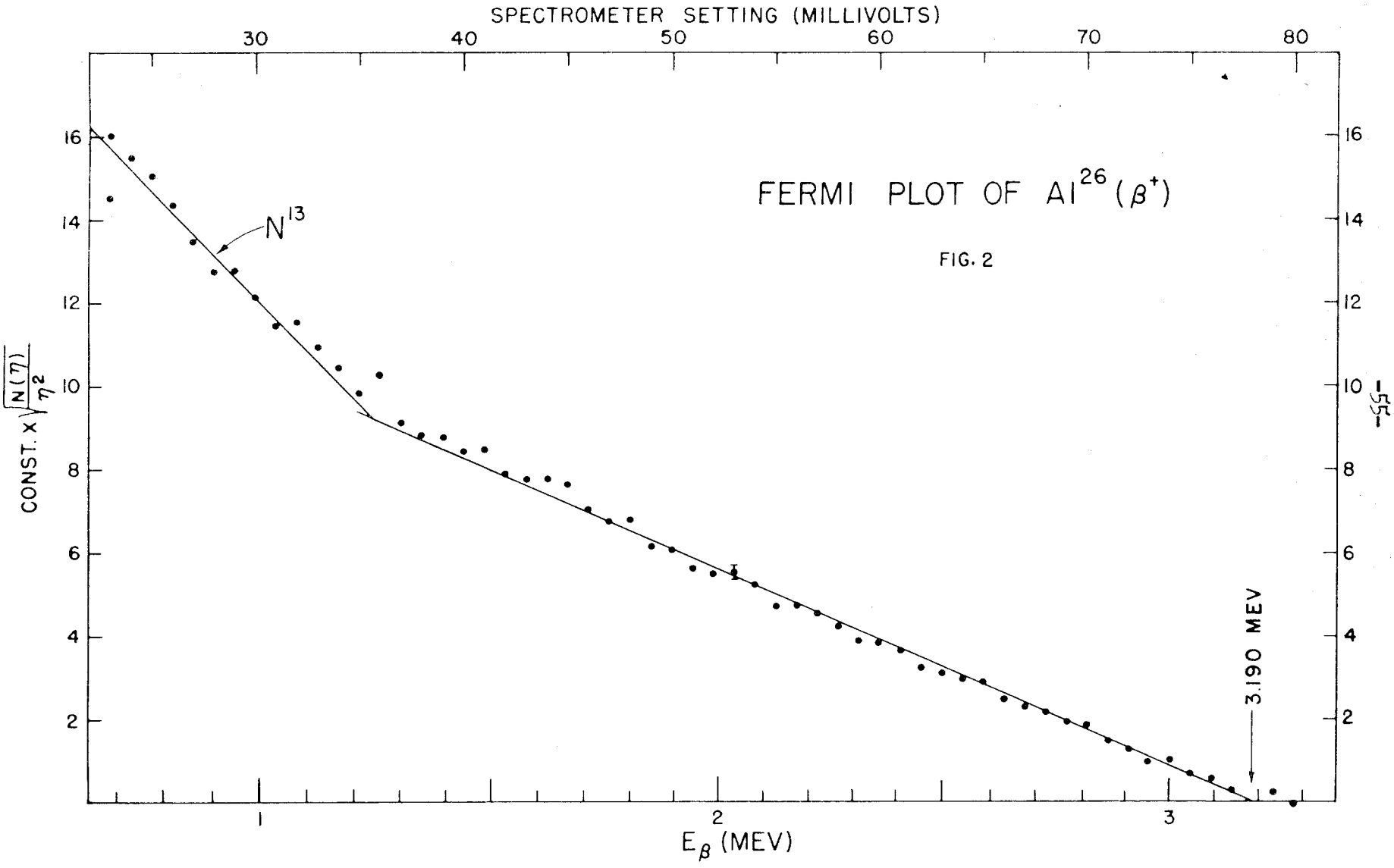
SPECTROMETER SETTING (MILLIVOLTS)
30
40
50
60
70
80
FERMI PLOT OF Al^{26} (β^+)
FIG. 2
N^{13}
3.190 MEV
CONST. x $\sqrt{\frac{N(\eta)}{\eta^2}}$
E_β (MEV)
1
2
3
2
4
6
8
10
12
14
16

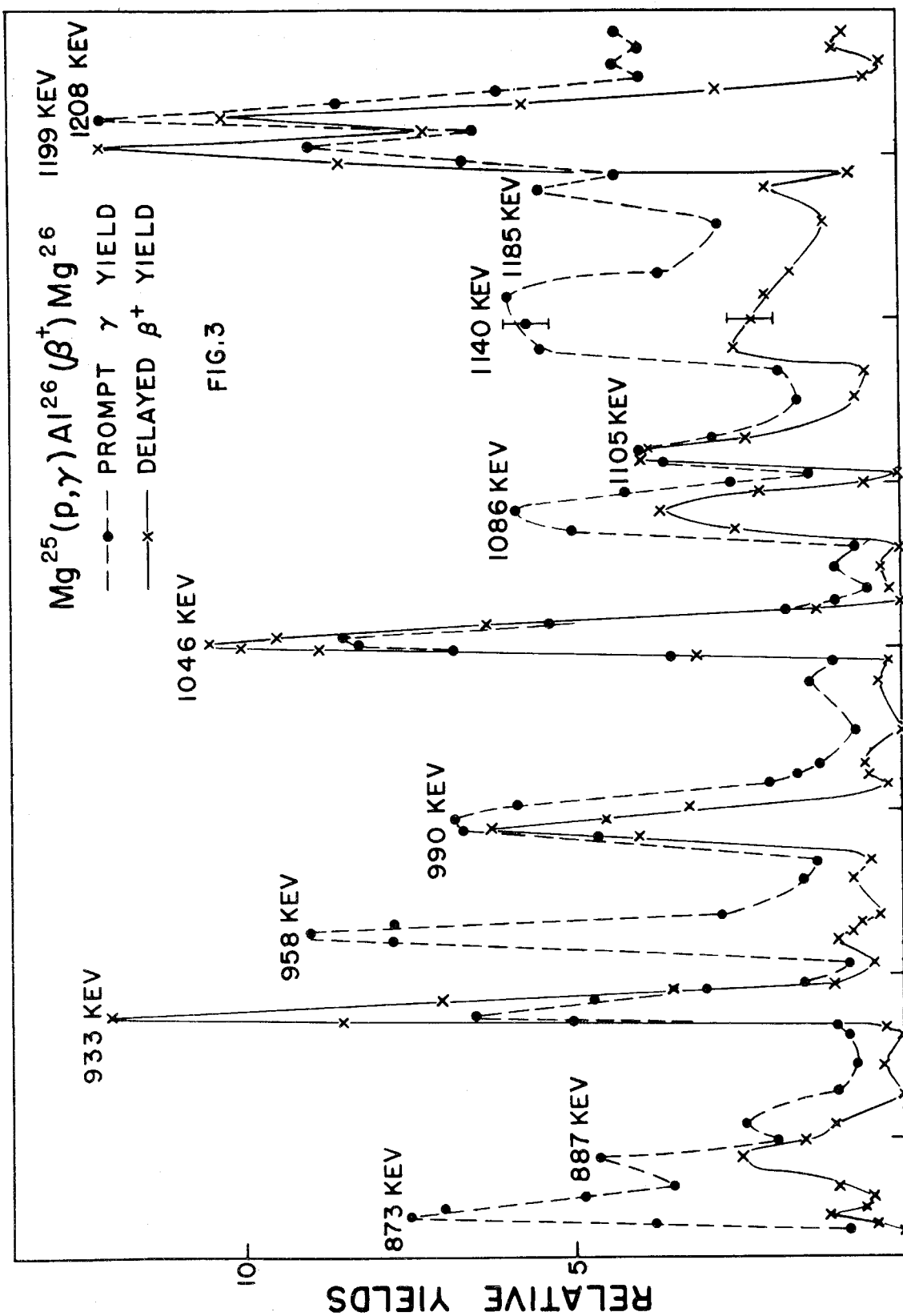
$Mg^{25}(p,\gamma)Al^{26}(\beta^+)Mg^{26}$
PROMPT γ YIELD
DELAYED β^+ YIELD
RELATIVE YIELDS
10
5
873 KEV
887 KEV
933 KEV
958 KEV
990 KEV
1046 KEV
1086 KEV
1105 KEV
1140 KEV
1185 KEV
1199 KEV
1208 KEV
900
1000
1100
1200
E_P in KEV

FIG.3

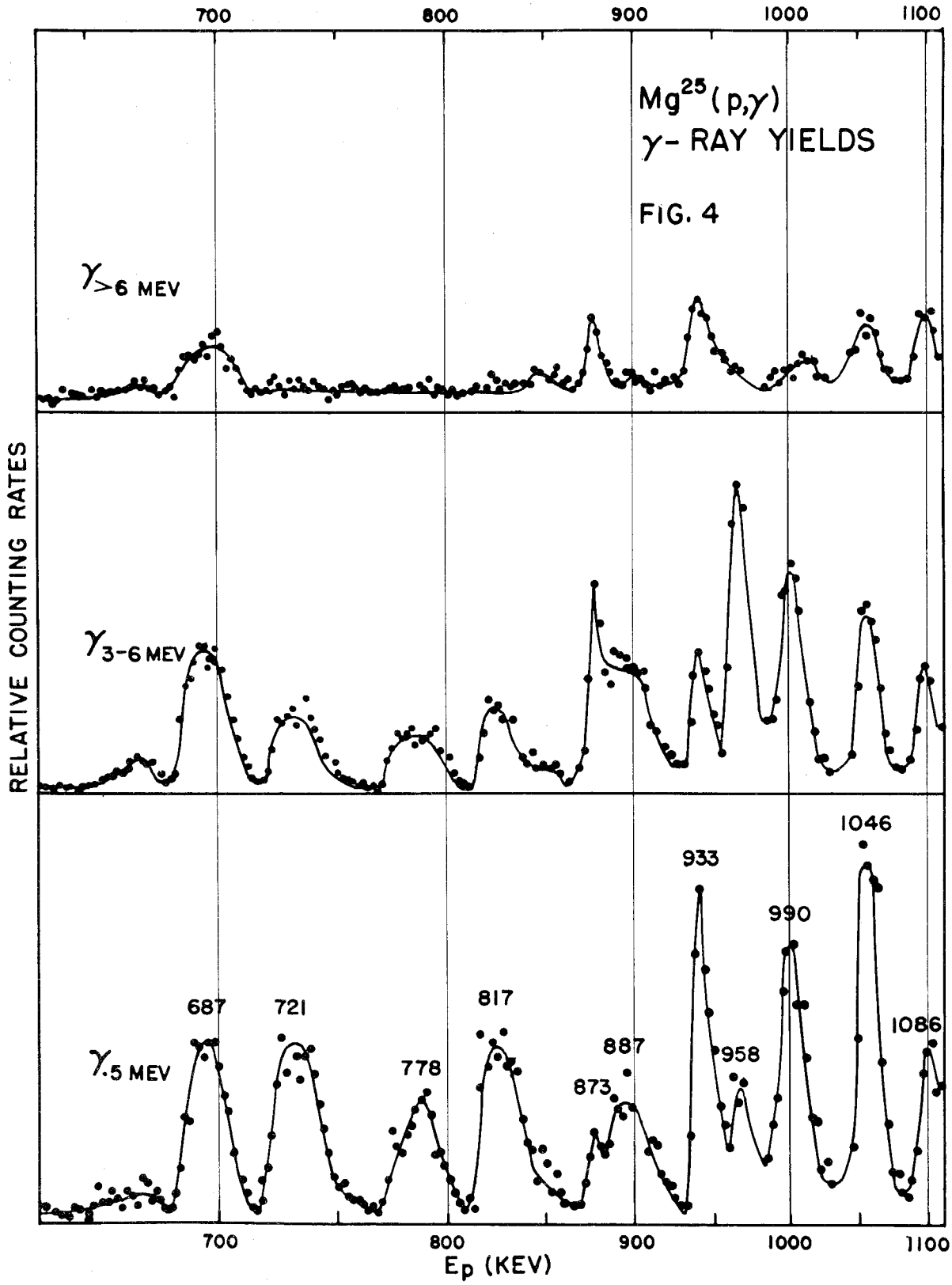
700
800
900
1000
1100
$Mg^{25}(p,\gamma)$
γ- RAY YIELDS
FIG. 4
$\gamma_{>6\ MEV}$
$\gamma_{3-6\ MEV}$
$\gamma_{.5\ MEV}$
RELATIVE COUNTING RATES
687
721
778
817
873
887
933
958
990
1046
1086
Ep (KEV)

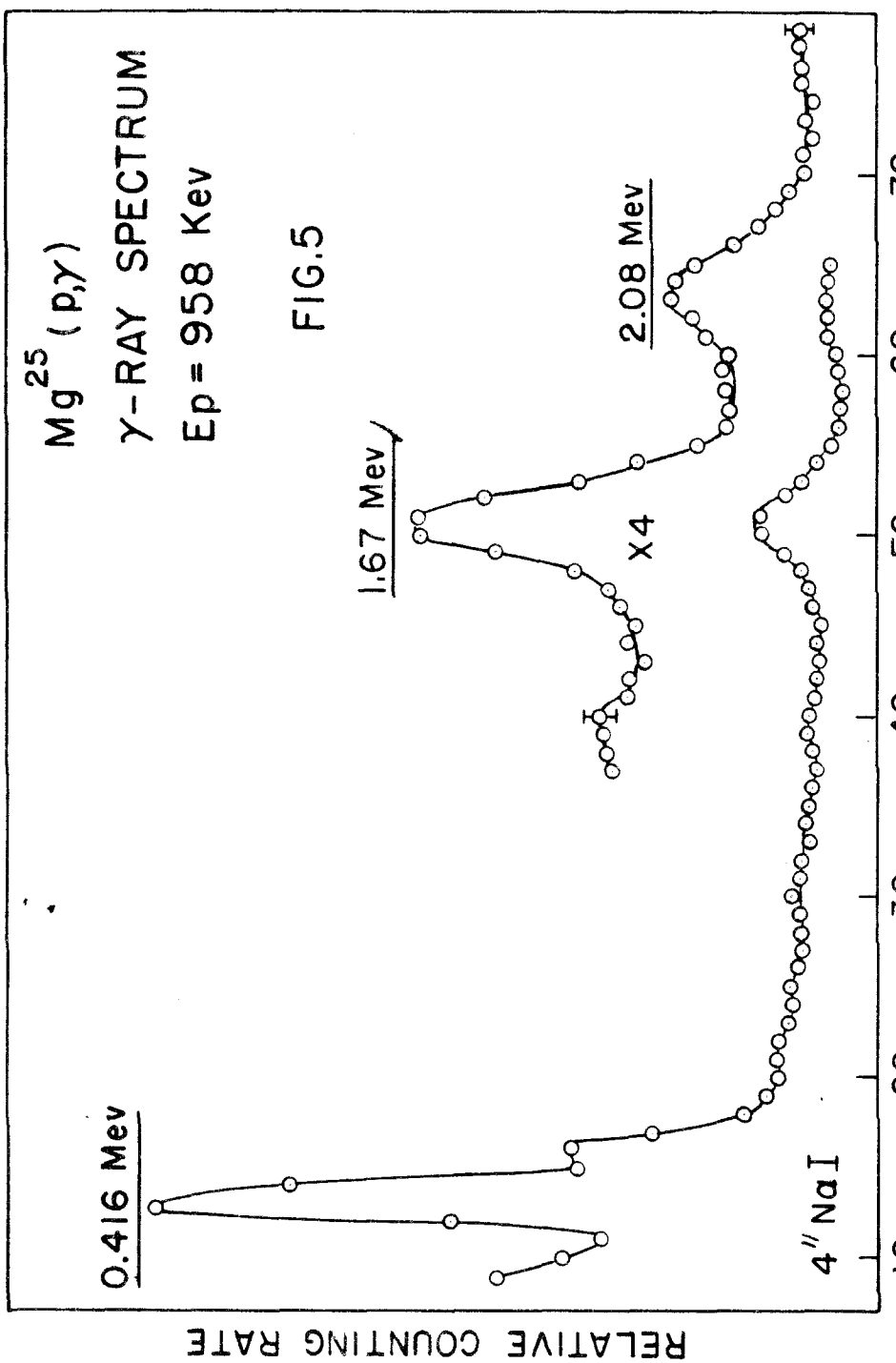
$Mg^{25}(p,\gamma)$
γ-RAY SPECTRUM
Ep = 958 Kev
FIG.5
0.416 Mev
1.67 Mev
2.08 Mev
X4
4" NaI
RELATIVE COUNTING RATE
PULSE HEIGHT
10
20
30
40
50
60
70

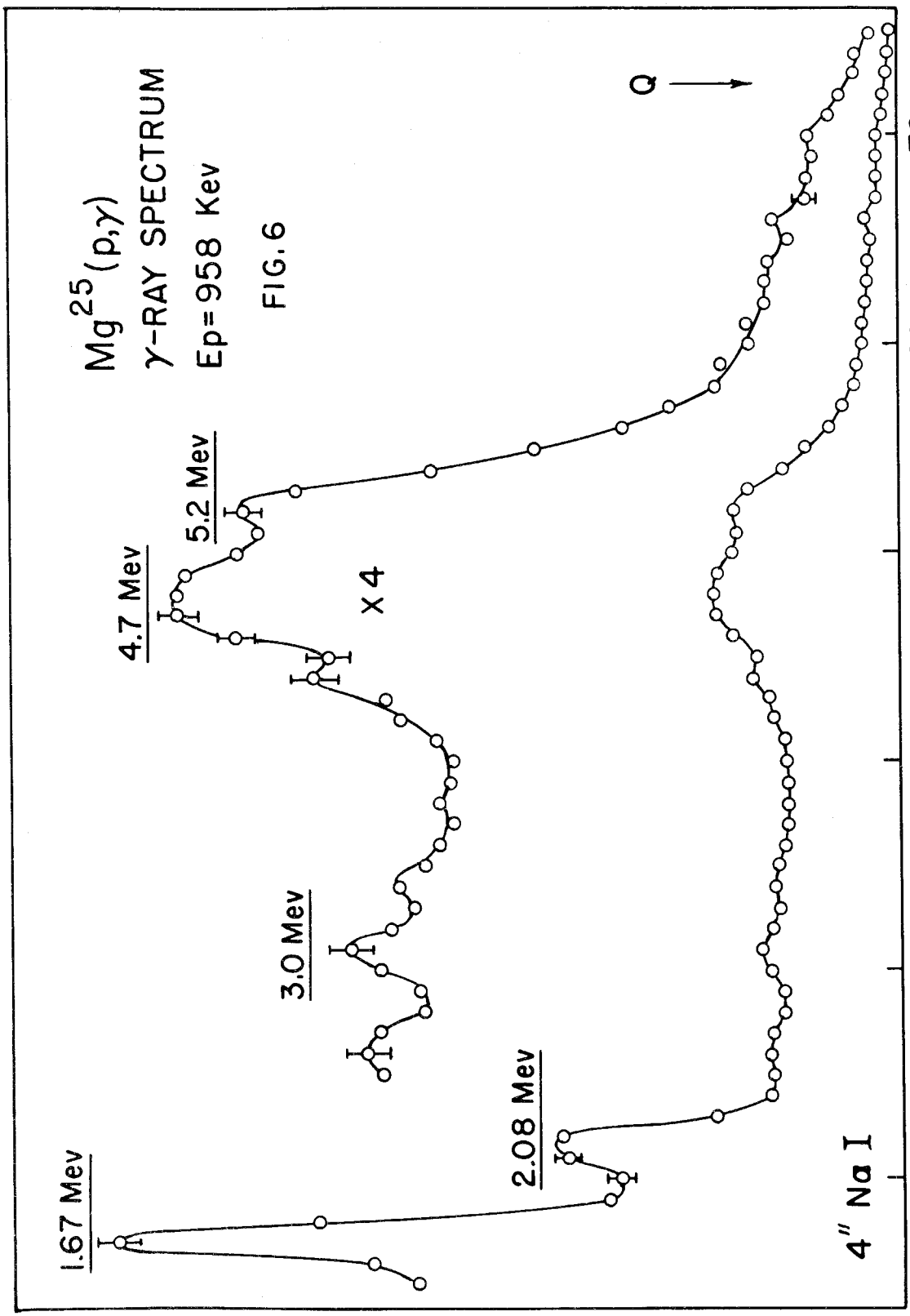
$Mg^{25}(p,\gamma)$
γ-RAY SPECTRUM
Ep=958 Kev
FIG. 6
1.67 Mev
2.08 Mev
3.0 Mev
4.7 Mev
5.2 Mev
X 4
Q
4" Na I
RELATIVE COUNTING RATE
PULSE HEIGHT
20
30
40
50
60
70

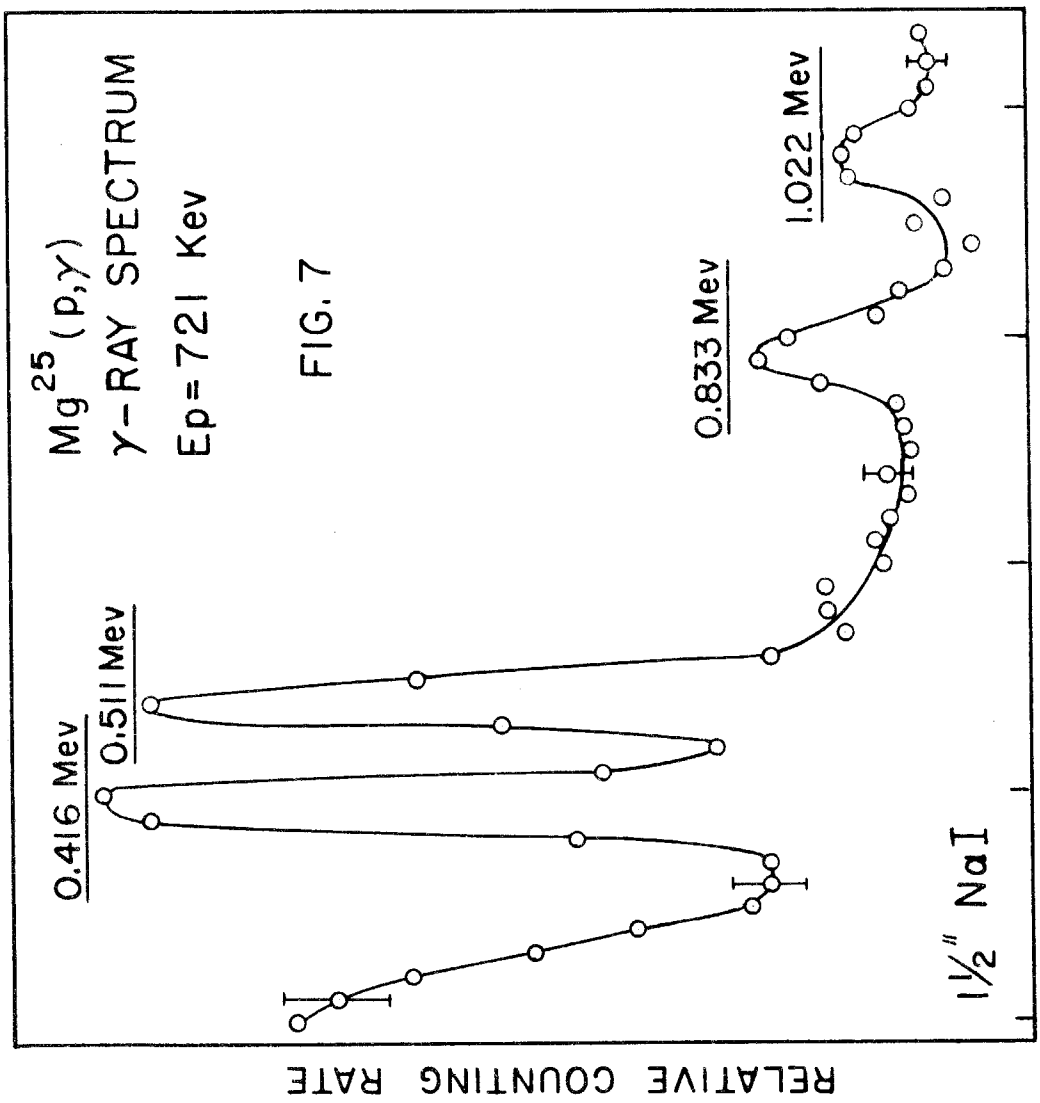
$Mg^{25}(p,\gamma)$
γ-RAY SPECTRUM
Ep = 721 Kev
0.416 Mev
0.511 Mev
0.833 Mev
1.022 Mev
1½" NaI
RELATIVE COUNTING RATE
PULSE HEIGHT
10
20
30
40
50

FIG. 7

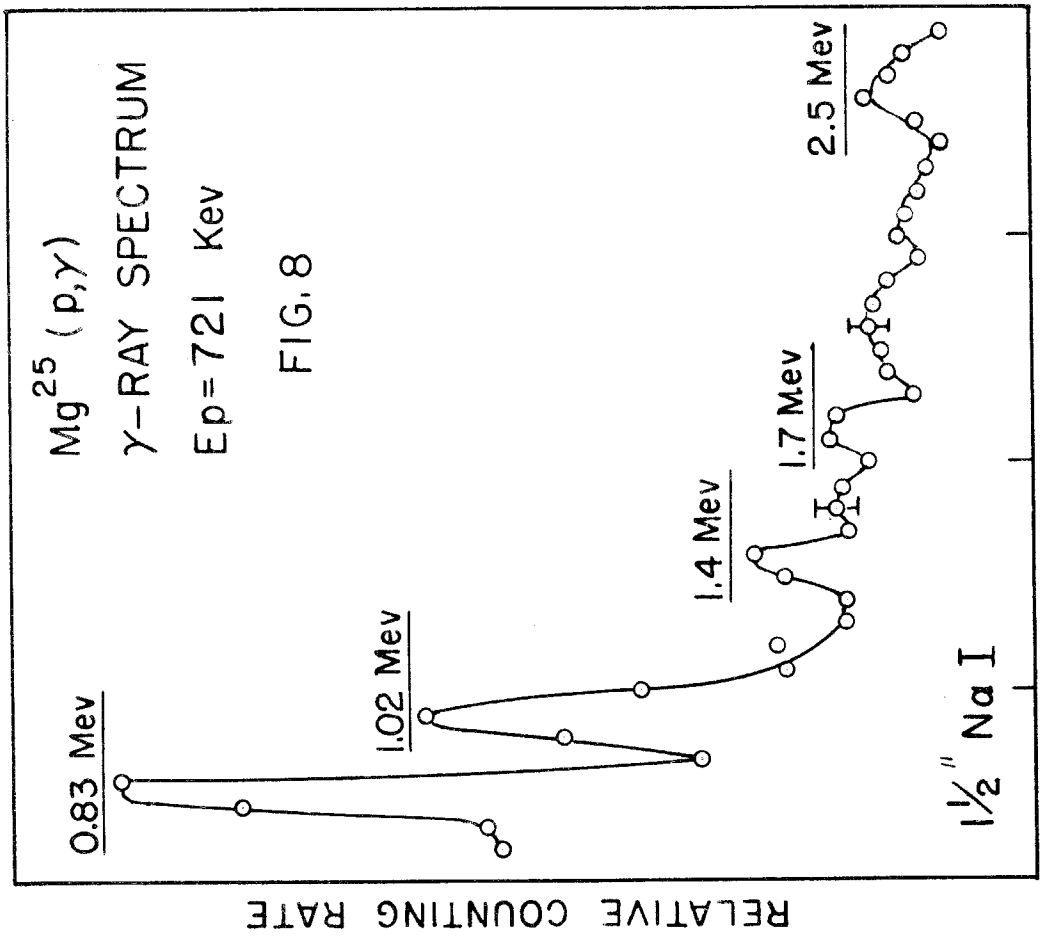
$Mg^{25}(p,\gamma)$
γ-RAY SPECTRUM
Ep=721 Kev
FIG. 8
0.83 Mev
1.02 Mev
1.4 Mev
1.7 Mev
2.5 Mev
1½" Na I
20
30
40
PULSE HEIGHT
RELATIVE COUNTING RATE

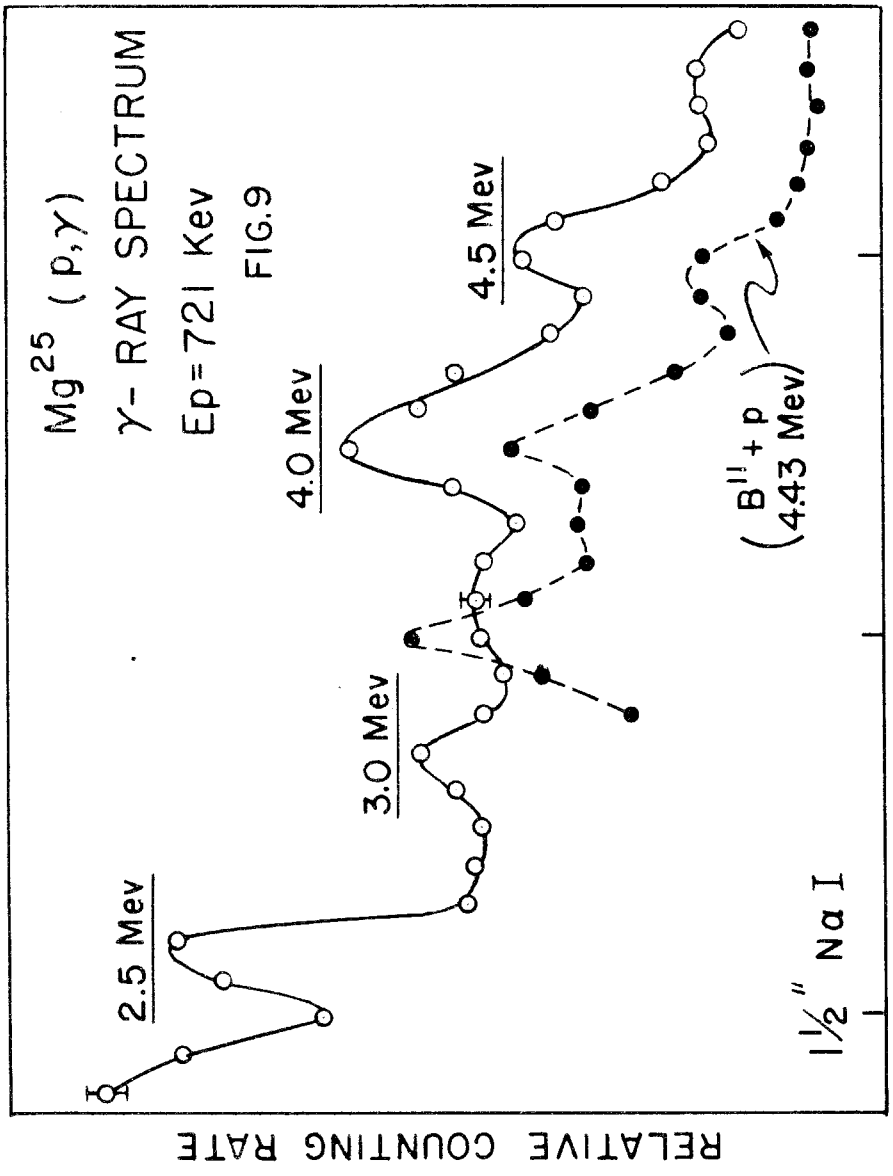
Mg^{25} (p,γ)
γ- RAY SPECTRUM
Ep=721 Kev
FIG.9
2.5 Mev
3.0 Mev
4.0 Mev
4.5 Mev
$(B^{11}+p$
(4.43 Mev)
1½" Na I
20
30
40
PULSE HEIGHT
RELATIVE COUNTING RATE

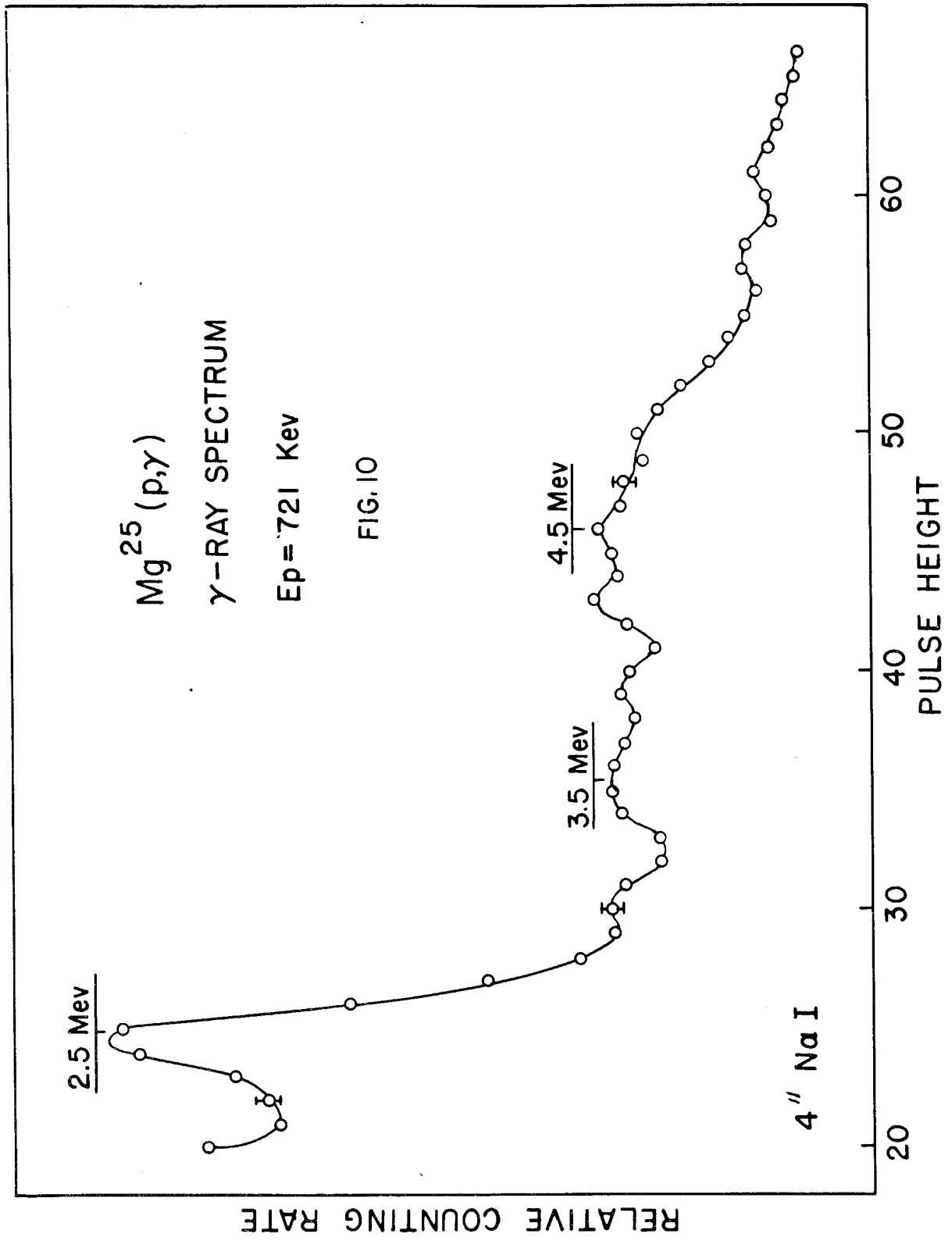
$Mg^{25}(p,\gamma)$
γ-RAY SPECTRUM
Ep=721 Kev
2.5 Mev
3.5 Mev
4.5 Mev
4" Na I
RELATIVE COUNTING RATE
PULSE HEIGHT
20
30
40
50
60

FIG. 10

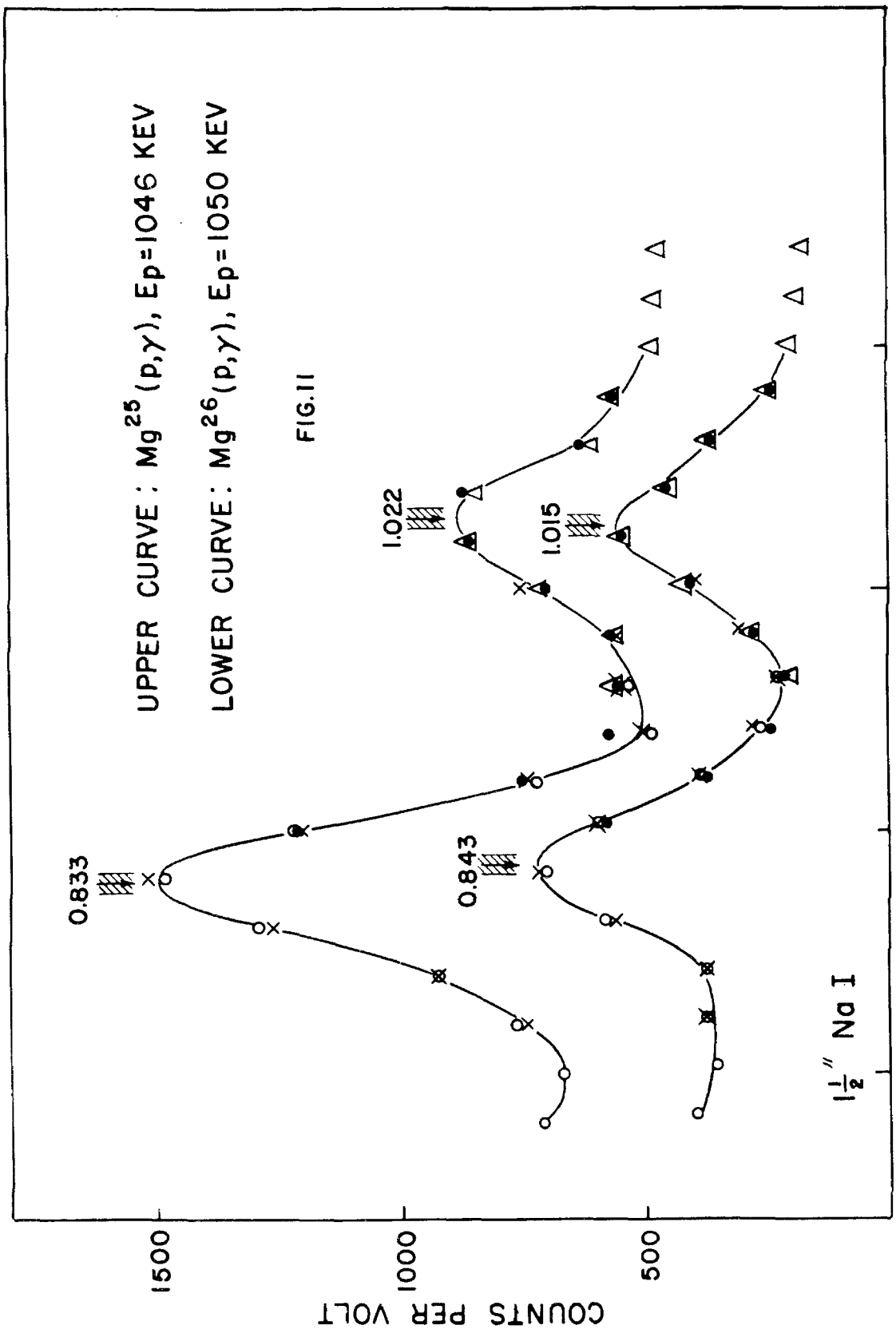
UPPER CURVE: $Mg^{25}(p,\gamma)$, Ep=1046 KEV
LOWER CURVE: $Mg^{26}(p,\gamma)$, Ep=1050 KEV
0.833
0.843
1.022
1.015
1500
1000
500
COUNTS PER VOLT
30
40
PULSE HEIGHT
$1\frac{1}{2}$" Na I

FIG. 11

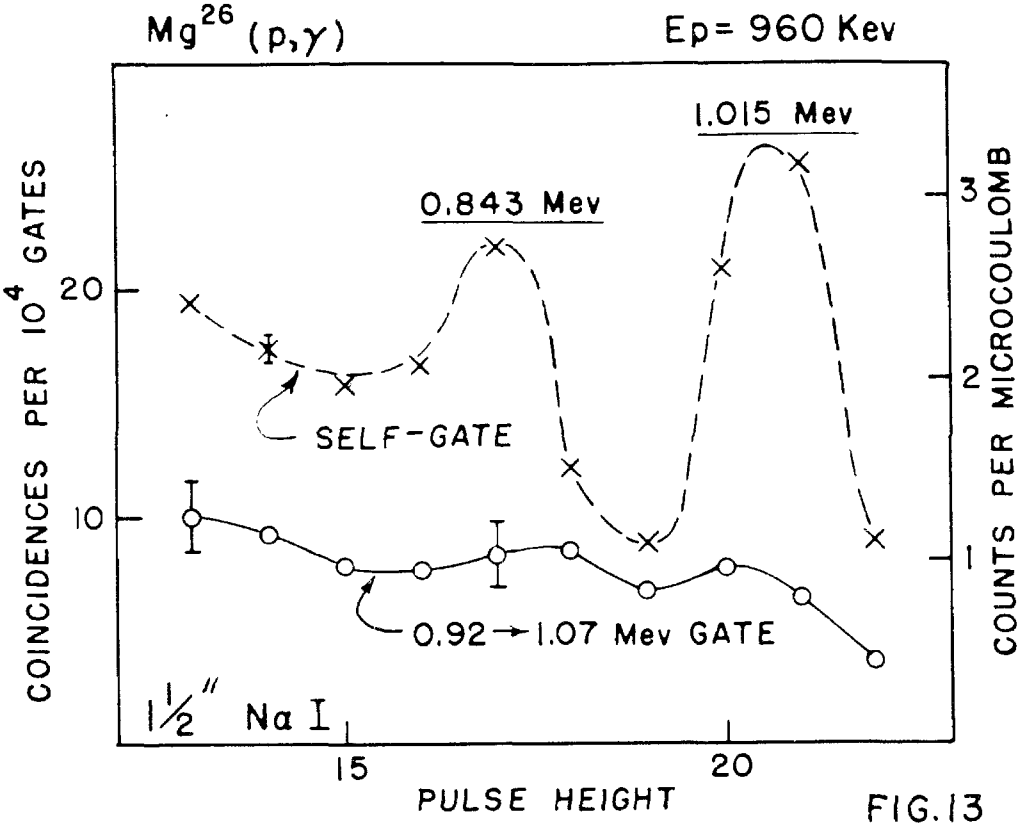
Mg26 (p,γ)
Ep= 960 Kev
1.015 Mev
0.843 Mev
SELF-GATE
0.92→1.07 Mev GATE
1½" NaI
COINCIDENCES PER 10⁴ GATES
COUNTS PER MICROCOULOMB
PULSE HEIGHT
20
10
15
20
3
2
1

FIG.13

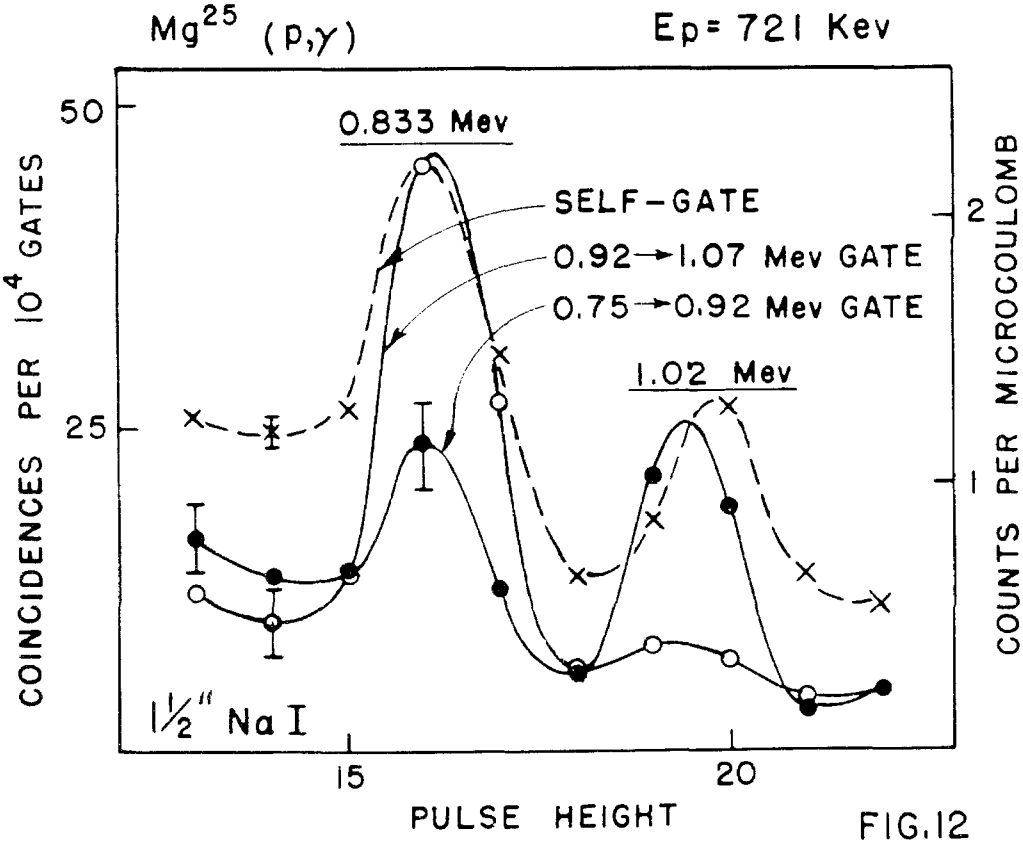
Mg25 (p,γ)
Ep= 721 Kev
0.833 Mev
SELF-GATE
0.92→1.07 Mev GATE
0.75→0.92 Mev GATE
1.02 Mev
1½" NaI
COINCIDENCES PER 10⁴ GATES
COUNTS PER MICROCOULOMB
PULSE HEIGHT
50
25
15
20
2
1

FIG.12

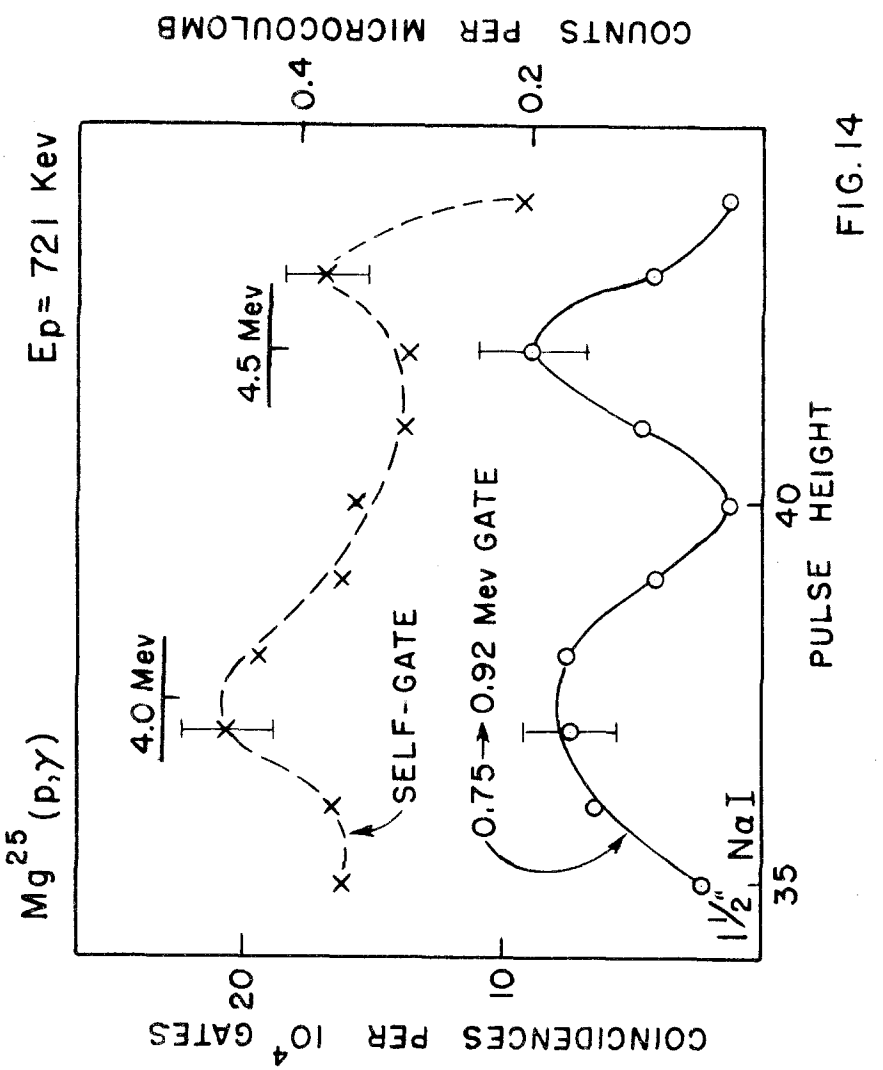
Mg25 (p,γ)
Ep= 721 Kev
4.0 Mev
4.5 Mev
SELF-GATE
0.75→0.92 Mev GATE
1½" NaI
COINCIDENCES PER 10⁴ GATES
COUNTS PER MICROCOULOMB
PULSE HEIGHT
0.4
0.2
20
10
35
40

FIG. 14

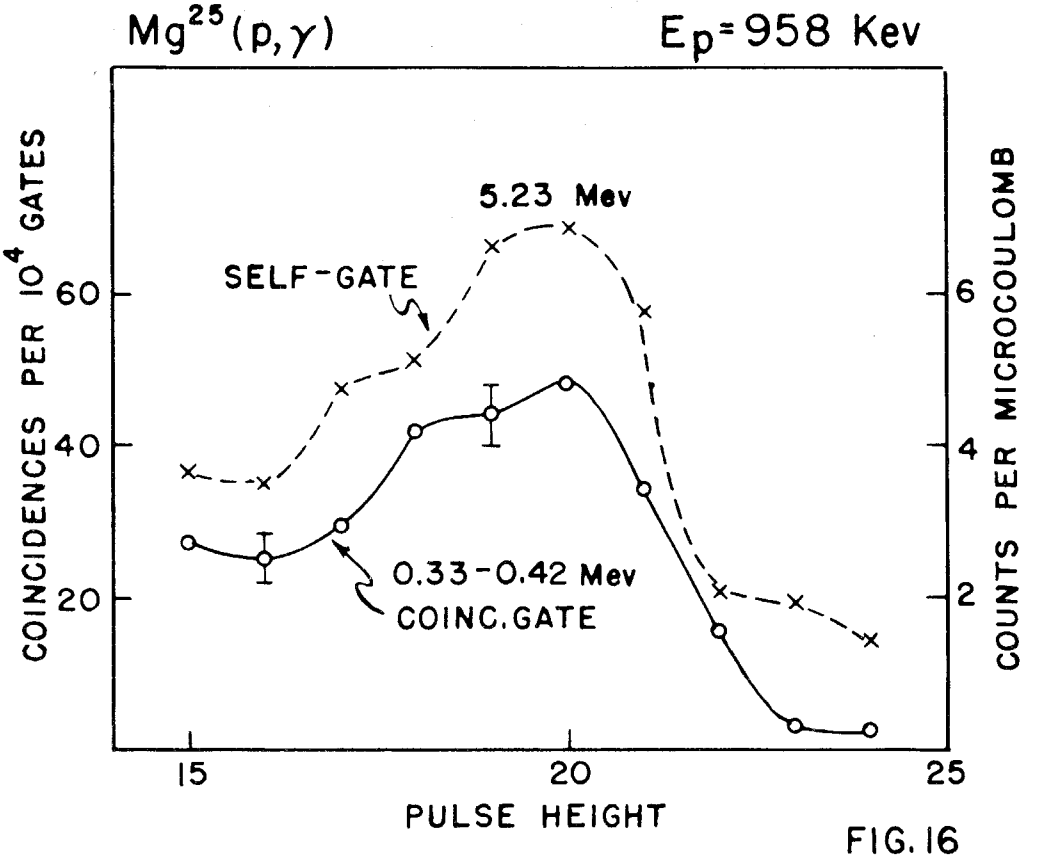
Mg25(p,γ)
Ep=958 Kev
5.23 Mev
SELF-GATE
0.33-0.42 Mev
COINC.GATE
COINCIDENCES PER 10^4 GATES
COUNTS PER MICROCOULOMB
PULSE HEIGHT
60
40
20
6
4
2
15
20
25

FIG. 16

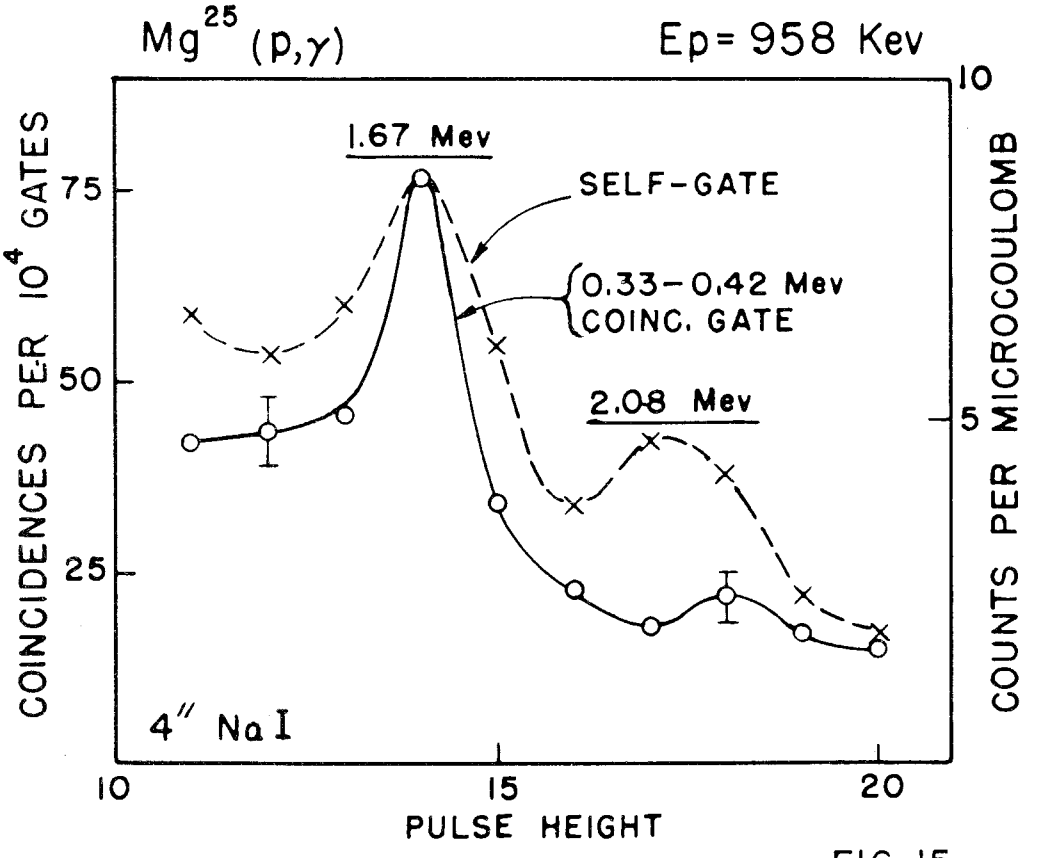
Mg25 (p,γ)
Ep= 958 Kev
1.67 Mev
SELF-GATE
0.33-0.42 Mev
COINC. GATE
2.08 Mev
4" NaI
COINCIDENCES PER 10^4 GATES
COUNTS PER MICROCOULOMB
PULSE HEIGHT
75
50
25
10
5
10
15
20

FIG. 15

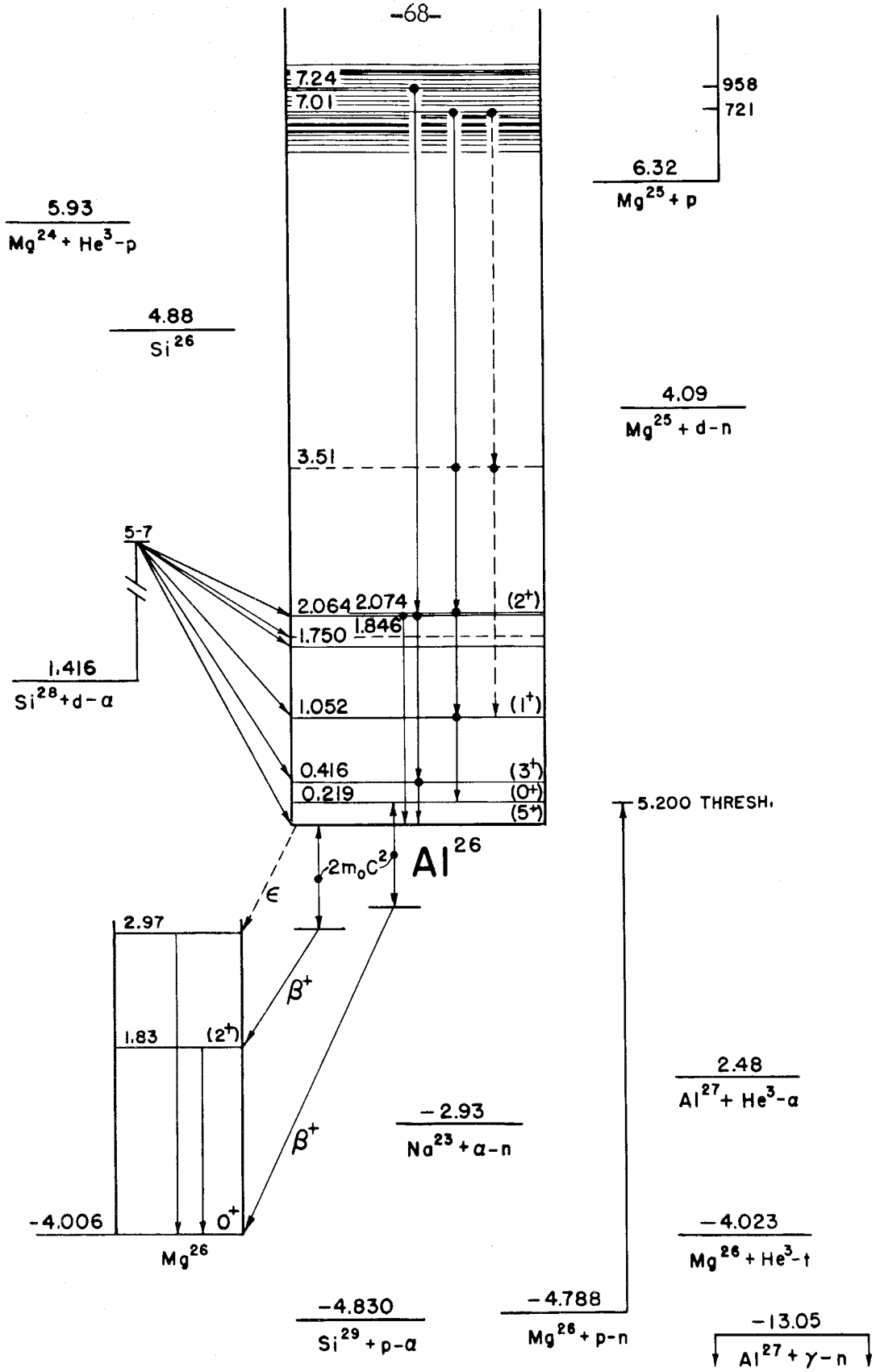
7.24
7.01
958
721
6.32
Mg25 + p
5.93
Mg24 + He3-p
4.88
Si26
4.09
Mg25 + d-n
3.51
5-7
2.064 2.074 (2+)
1.750 1.846
1.416
Si28+d-α
1.052 (1+)
0.416 (3+)
0.219 (0+)
(5+)
5.200 THRESH.
2moc2
Al26
ε
2.97
β+
1.83 (2+)
β+
2.48
Al27+ He3-α
-2.93
Na23 + α-n
-4.006 0+
Mg26
-4.023
Mg26 + He3-t
-4.830
Si29 + p-α
-4.788
Mg26 + p-n
-13.05
Al27 + γ-n

FIG. 17

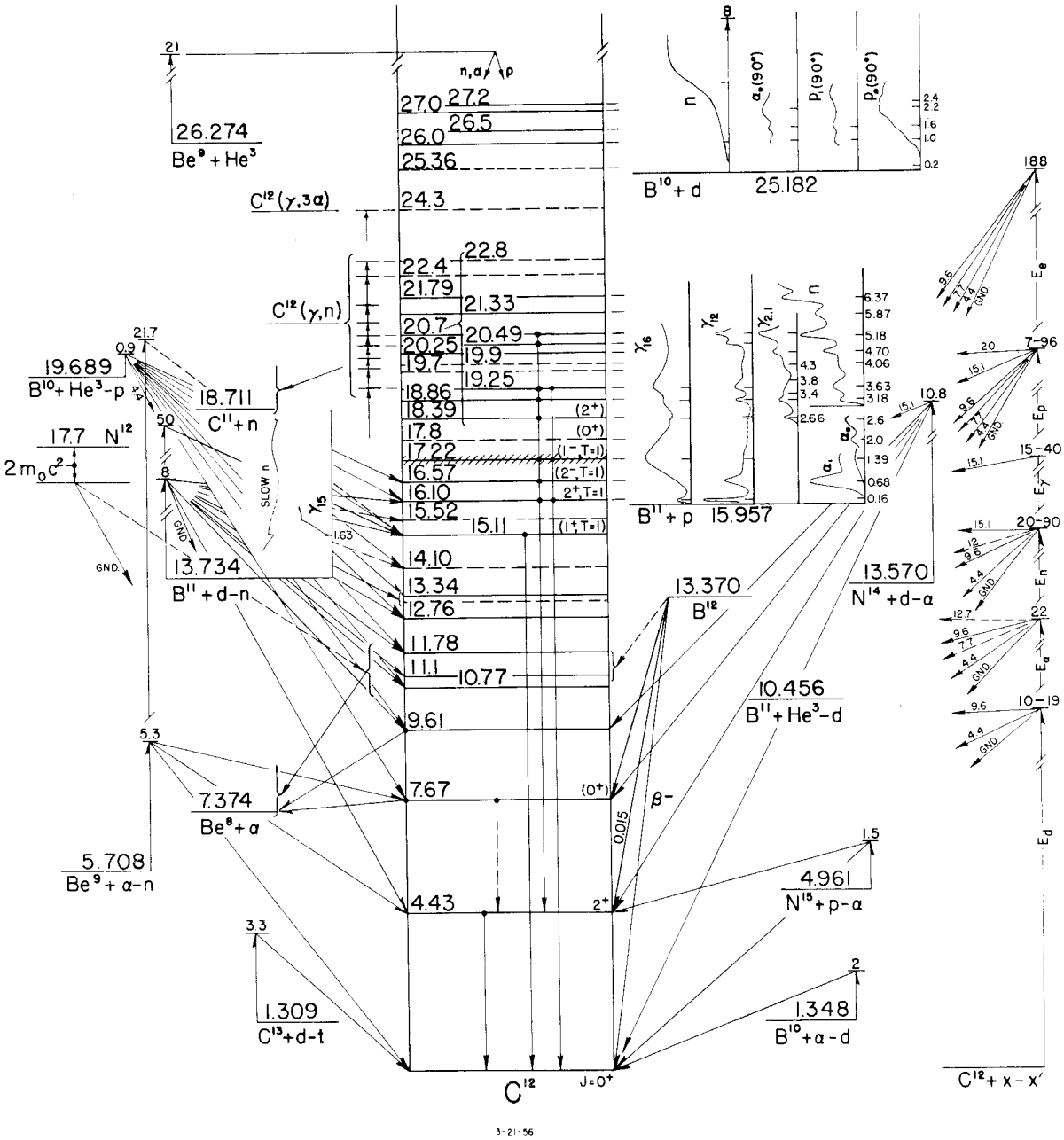
26.274
Be⁹ + He³
C¹²(γ,3α)
C¹²(γ,n)
19.689
B¹⁰+He³-p
17.7 N¹²
2m₀c²
18.711
C¹¹+n
13.734
B¹¹+d-n
5.708
Be⁹+α-n
7.374
Be⁸+α
1.309
C¹³+d-t
B¹⁰+d 25.182
B¹¹+p 15.957
13.370
B¹²
13.570
N¹⁴+d-α
10.456
B¹¹+He³-d
4.961
N¹⁵+p-α
1.348
B¹⁰+α-d
C¹²
J=0⁺
C¹²+x-x'
β-
0.015
SLOW n
GND
27.2
27.0
26.5
26.0
25.36
24.3
22.8
22.4
21.79
21.33
20.7
20.49
20.25
19.9
19.7
19.25
18.86
18.39
17.8
17.22
16.57
16.10
15.52
15.11
14.10
13.34
12.76
11.78
11.1
10.77
9.61
7.67
4.43
(2⁺)
(0⁺)
(1⁻,T=1)
(2⁻,T=1)
2⁺,T=1
(1⁺,T=1)
(0⁺)
2⁺
E_e
E_p
E_γ
E_n
E_α
E_d
7-96
15-40
20-90
10-19
22
188

FIG. 18

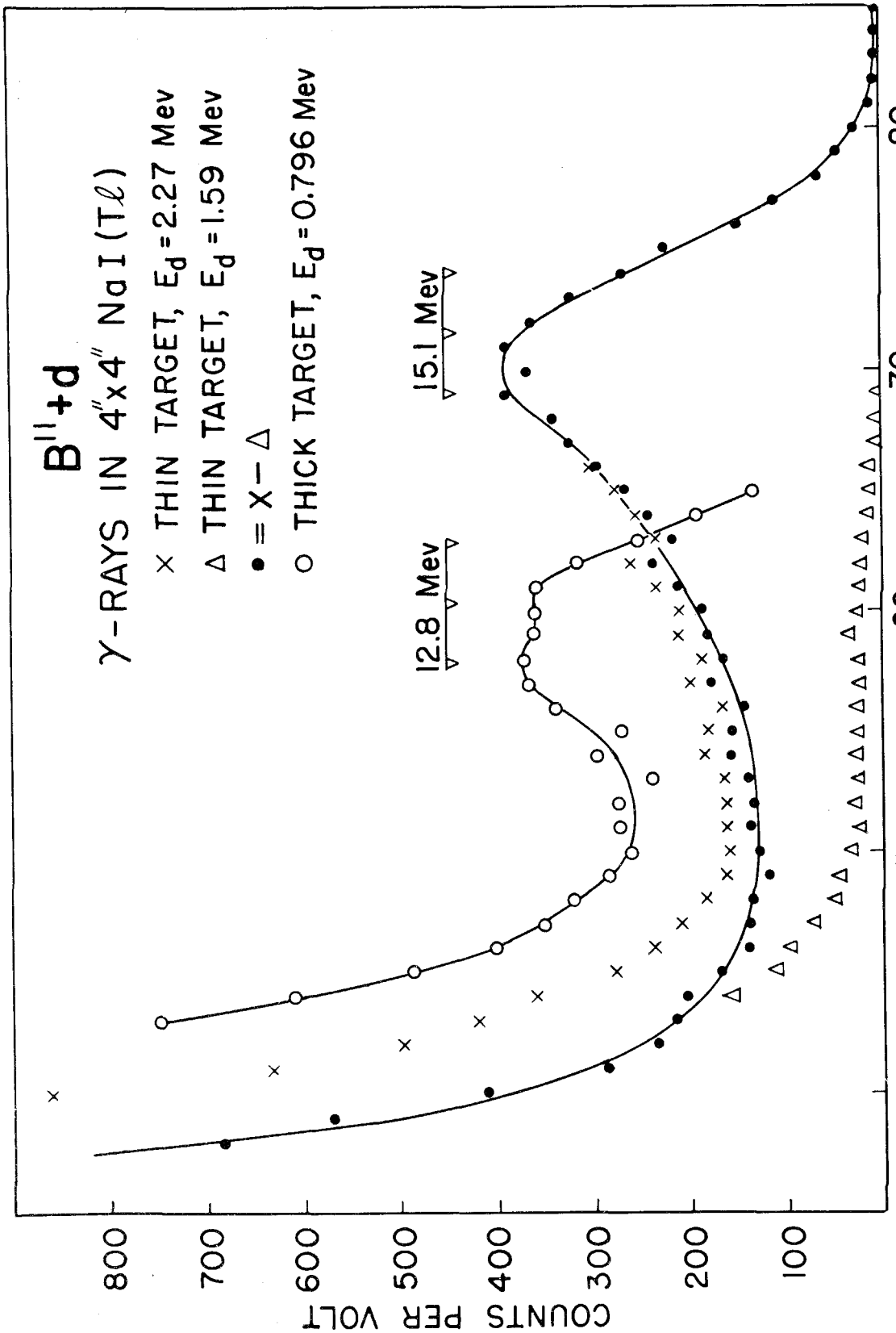
$B^{11}+d$
γ-RAYS IN 4"x4" NaI(Tℓ)
× THIN TARGET, E_d=2.27 Mev
Δ THIN TARGET, E_d=1.59 Mev
● = X − Δ
○ THICK TARGET, E_d=0.796 Mev
12.8 Mev
15.1 Mev
COUNTS PER VOLT
PULSE HEIGHT (VOLTS)
800
700
600
500
400
300
200
100
40
50
60
70
80

FIG. 19

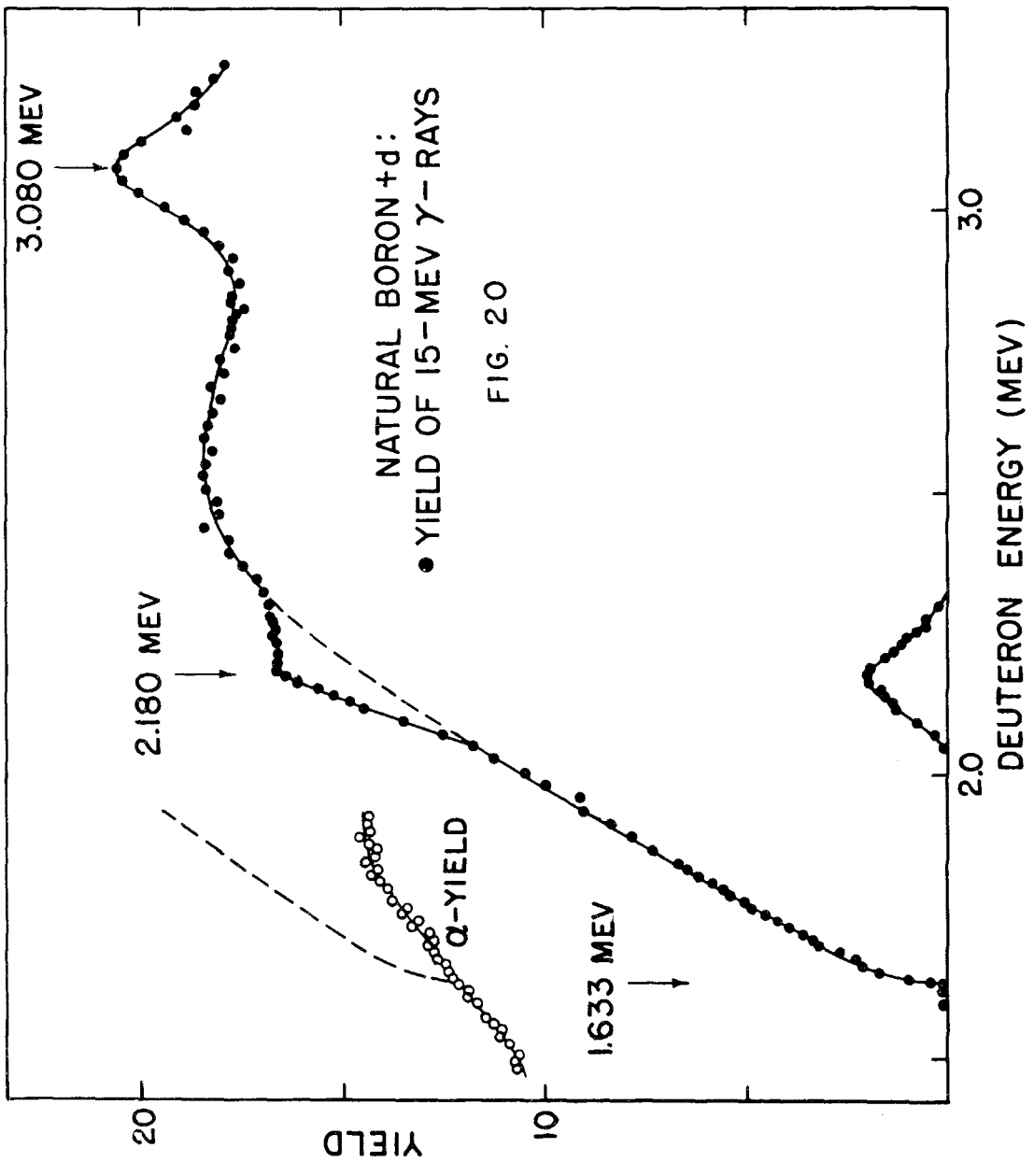
3.080 MEV
2.180 MEV
1.633 MEV
α-YIELD
NATURAL BORON + d:
● YIELD OF 15-MEV γ-RAYS
YIELD
20
10
2.0
3.0
DEUTERON ENERGY (MEV)

FIG. 20

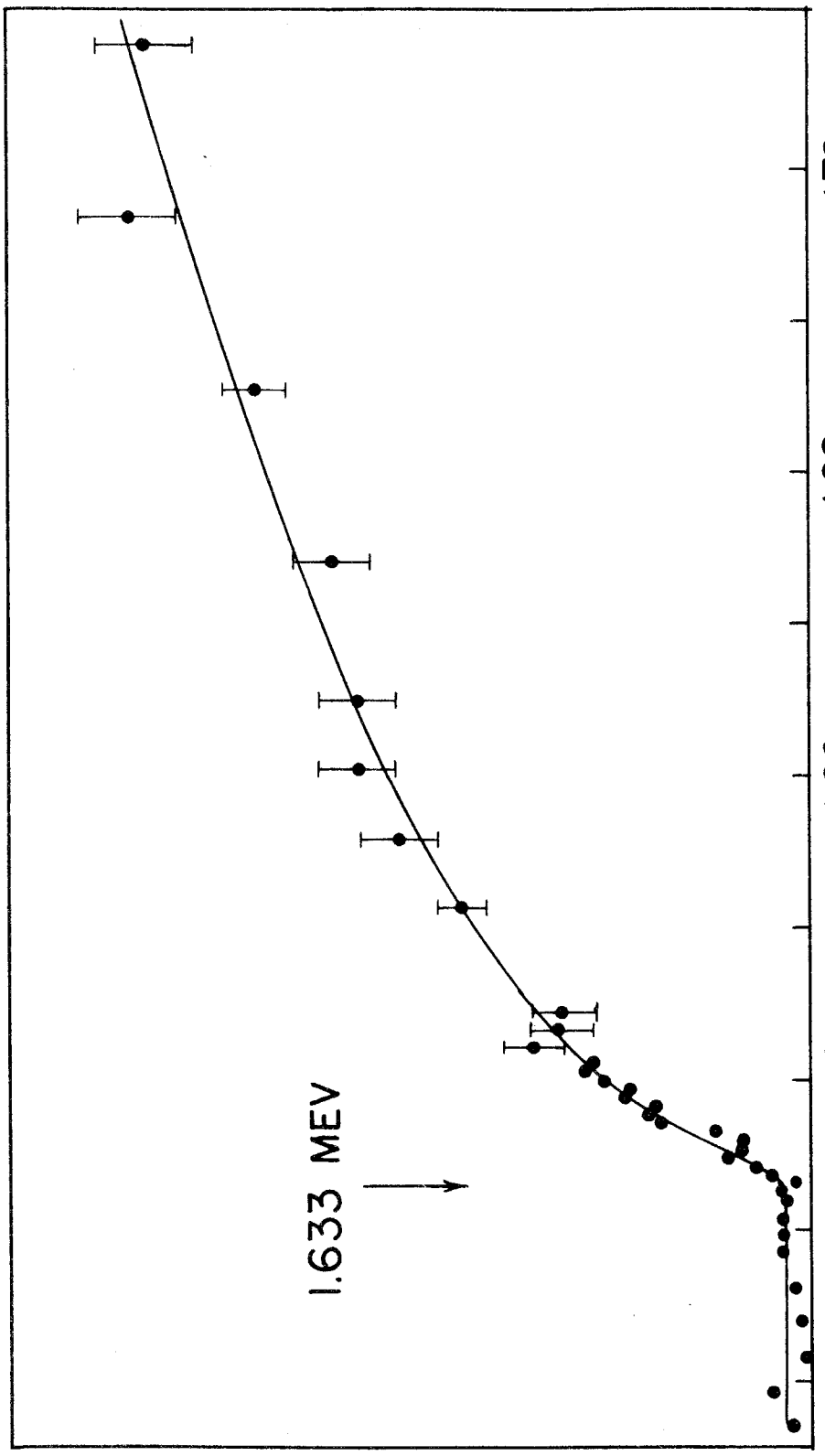
γ_{15}-YIELD
1.633 MEV
1.62
1.64
1.66
1.68
1.70
DEUTERON ENERGY (MEV)

FIG. 21

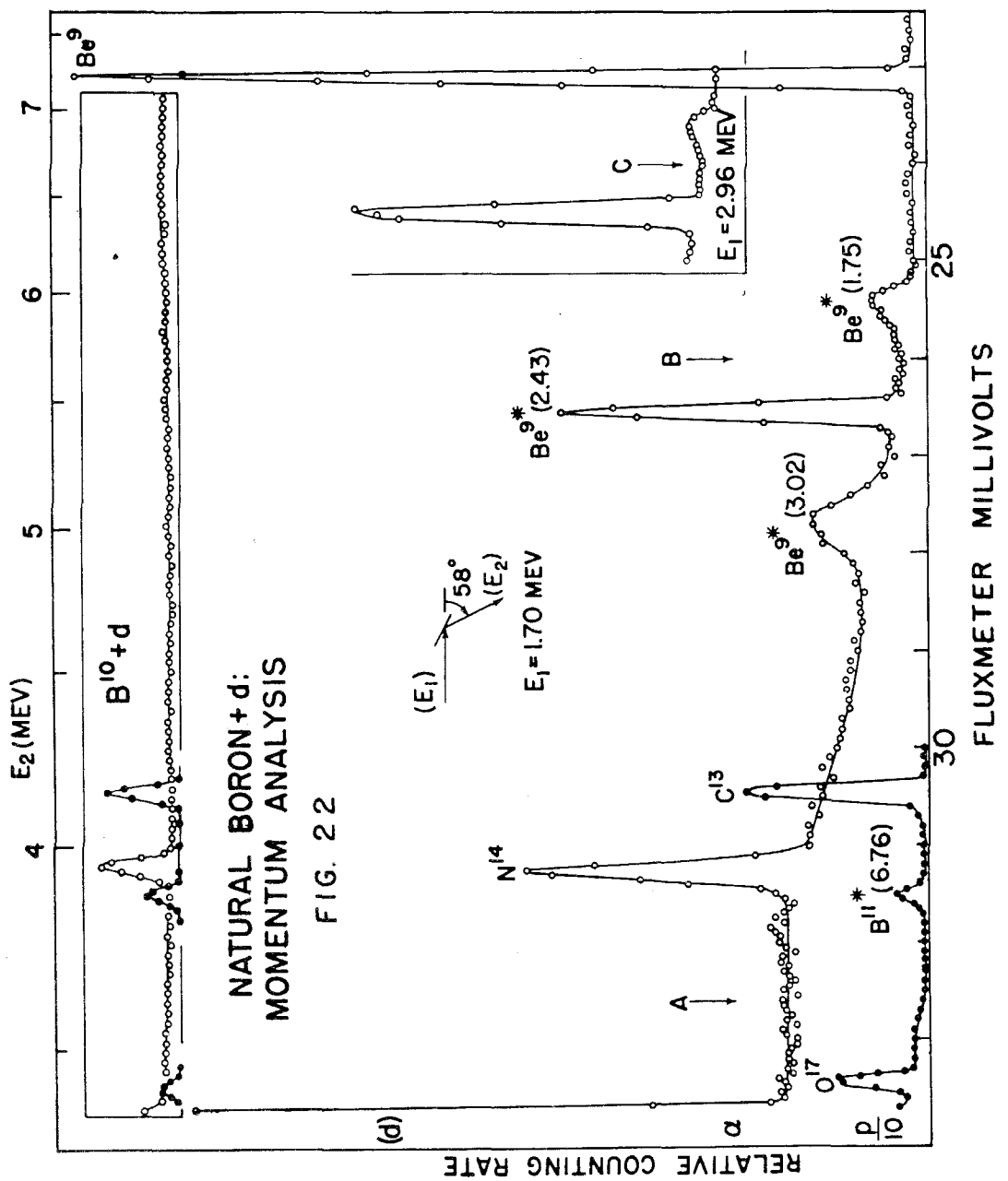
NATURAL BORON + d:
MOMENTUM ANALYSIS
FIG. 22
RELATIVE COUNTING RATE
FLUXMETER MILLIVOLTS
E2 (MEV)
4
5
6
7
25
30
(d)
α
p/10
B10+d
Be9
N14
C13
O17
B11* (6.76)
A
(E1)
58°
(E2)
E1=1.70 MEV
Be9* (2.43)
Be9* (3.02)
B
C
E1=2.96 MEV
Be9* (1.75)

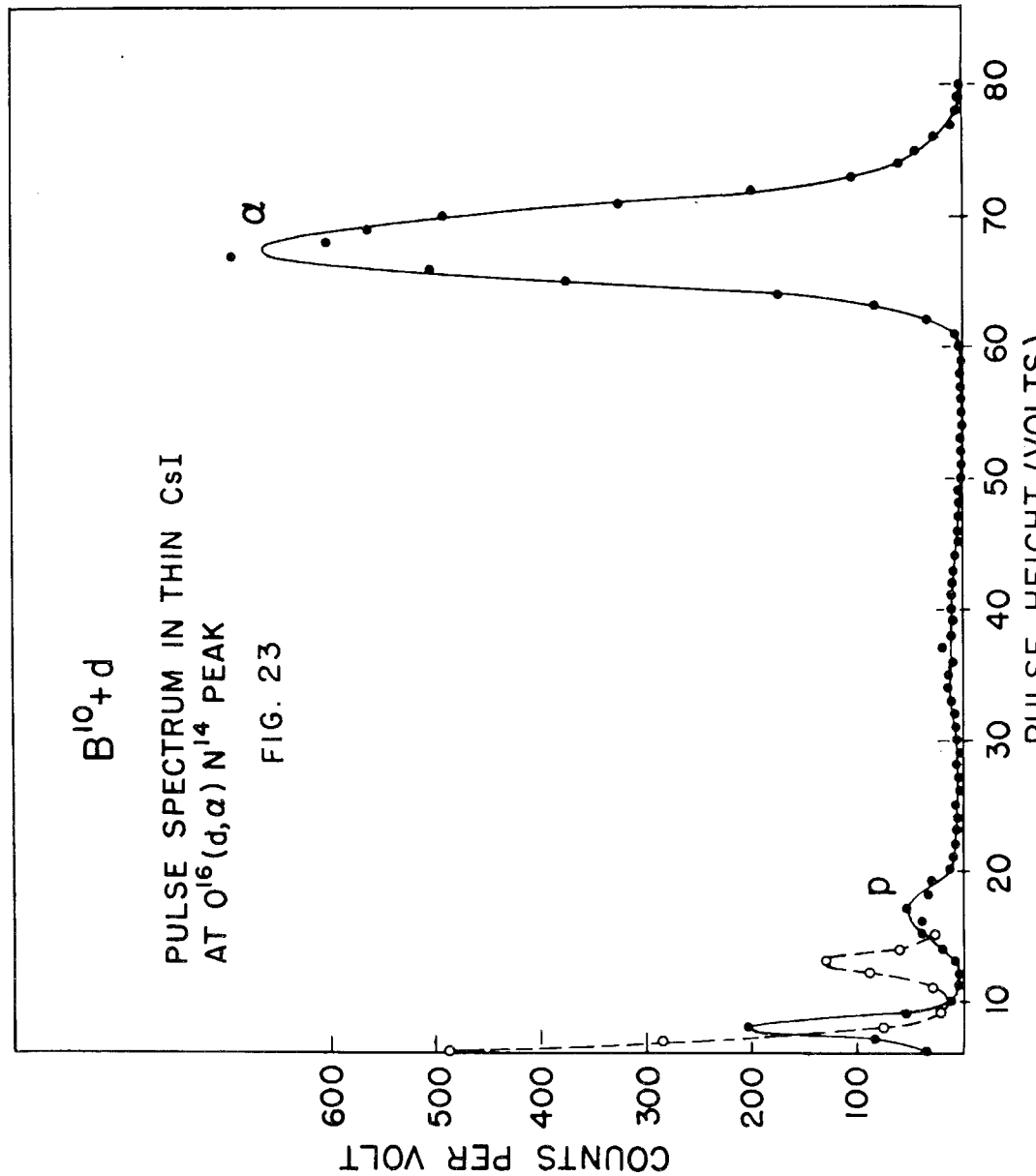
$B^{10}+d$
PULSE SPECTRUM IN THIN CsI
AT $O^{16}(d,\alpha)N^{14}$ PEAK
α
p
A
COUNTS PER VOLT
100
200
300
400
500
600
10
20
30
40
50
60
70
80
PULSE HEIGHT (VOLTS)

FIG. 23

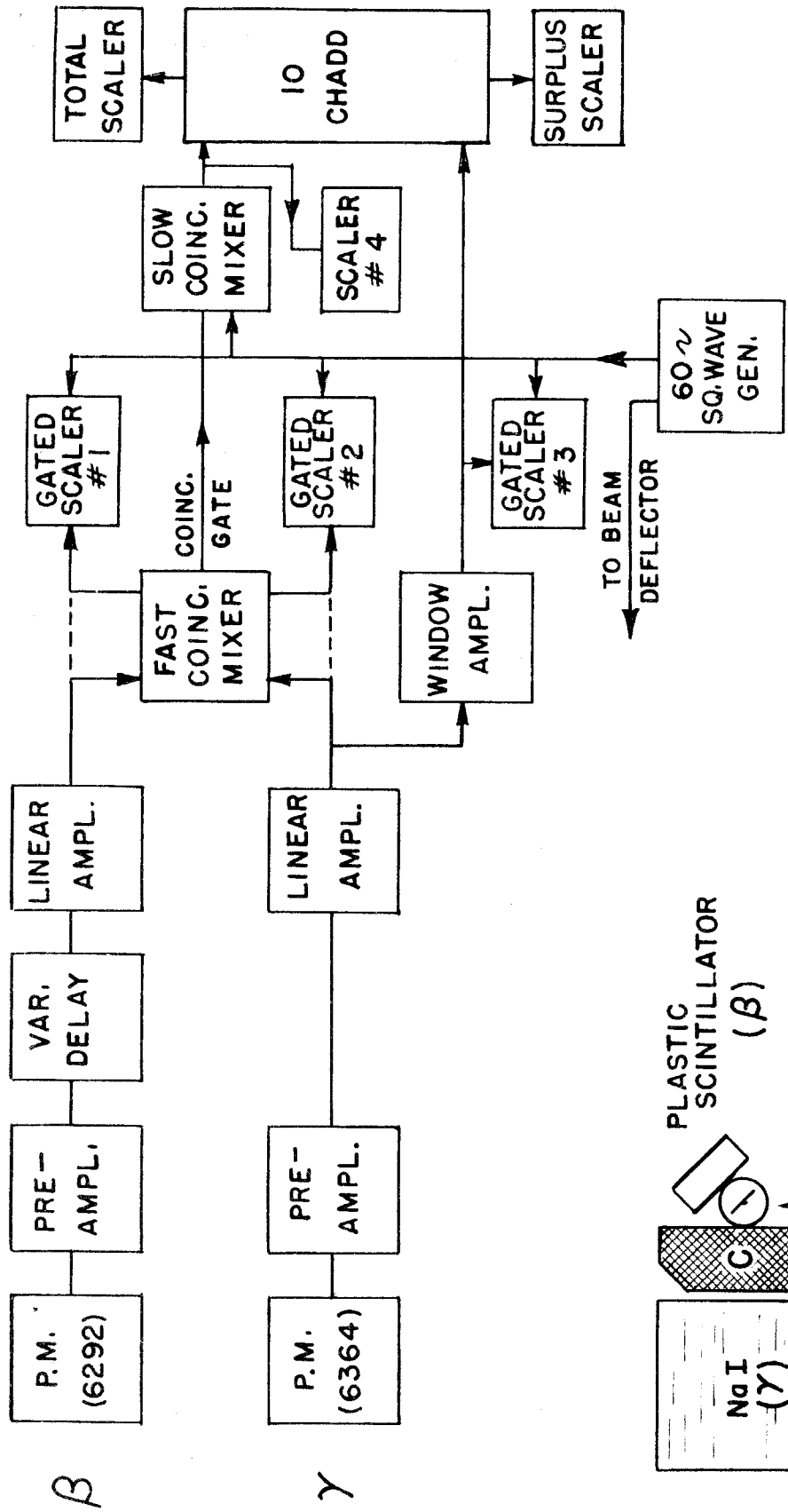
TOTAL SCALER
IO CHADD
SURPLUS SCALER
SLOW COINC. MIXER
SCALER #4
60~ SQ. WAVE GEN.
GATED SCALER #1
COINC. GATE
GATED SCALER #2
GATED SCALER #3
TO BEAM DEFLECTOR
FAST COINC. MIXER
WINDOW AMPL.
LINEAR AMPL.
LINEAR AMPL.
VAR. DELAY
PRE-AMPL.
PRE-AMPL.
P.M. (6292)
P.M. (6364)
β
γ
PLASTIC SCINTILLATOR (β)
DEUTERON BEAM
C
NaI (γ)

FIG. 24

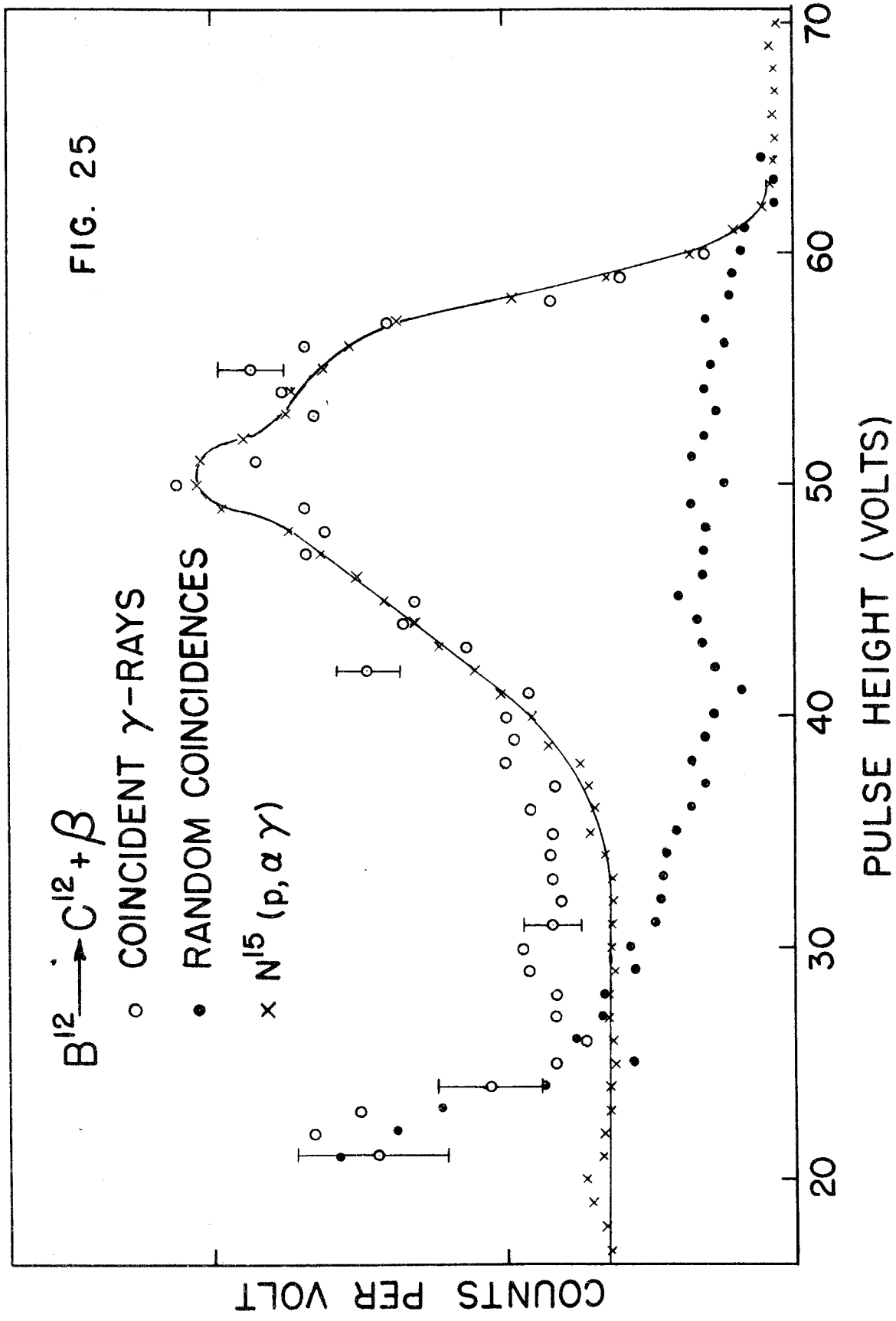
FIG. 25
$B^{12} \rightarrow C^{12} + \beta$
○ COINCIDENT γ-RAYS
● RANDOM COINCIDENCES
× $N^{15}(p, \alpha\gamma)$
COUNTS PER VOLT
PULSE HEIGHT (VOLTS)
20
30
40
50
60
70

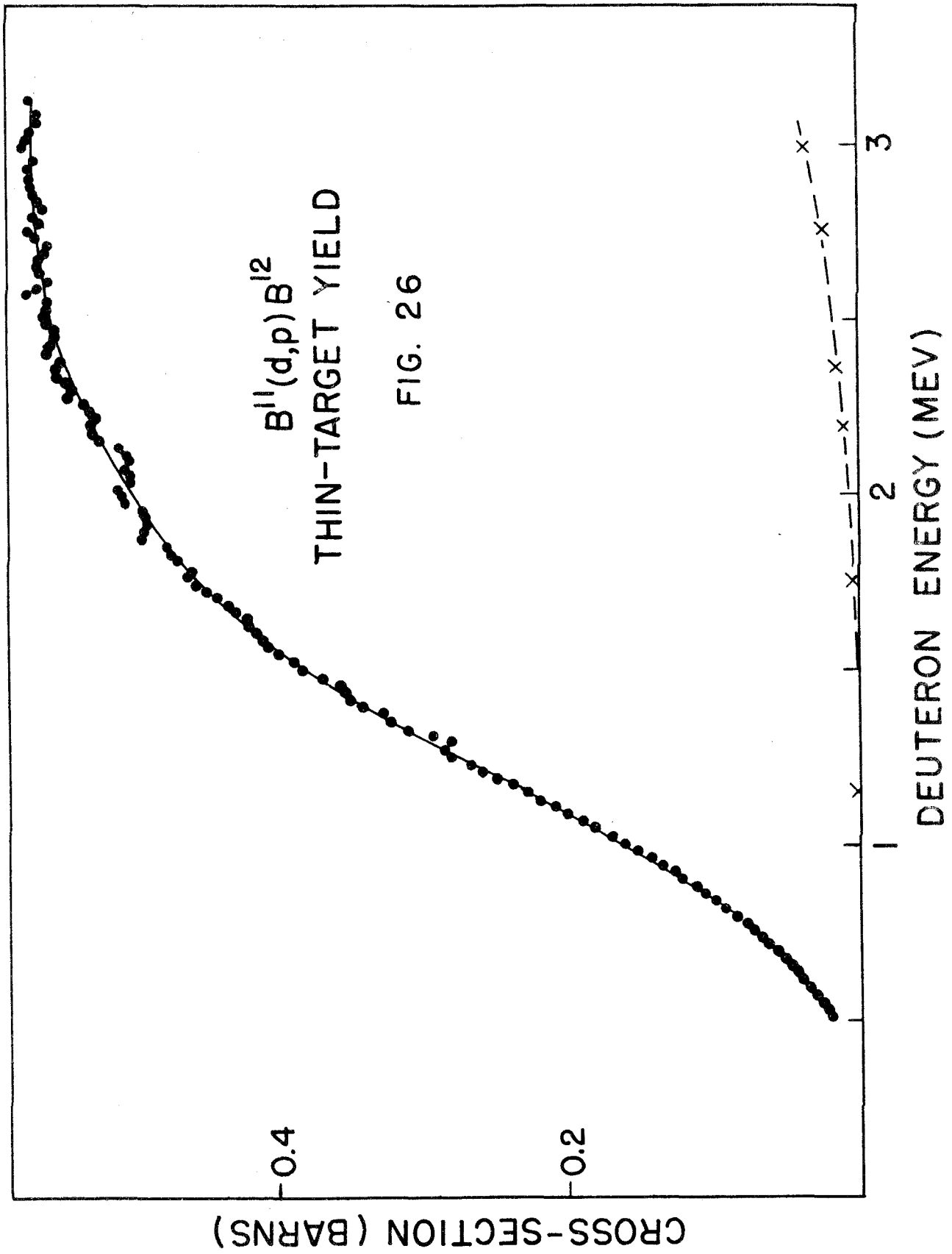
$B^{11}(d,p)B^{12}$
THIN-TARGET YIELD
FIG. 26
CROSS-SECTION (BARNS)
0.4
0.2
1
2
3
DEUTERON ENERGY (MEV)

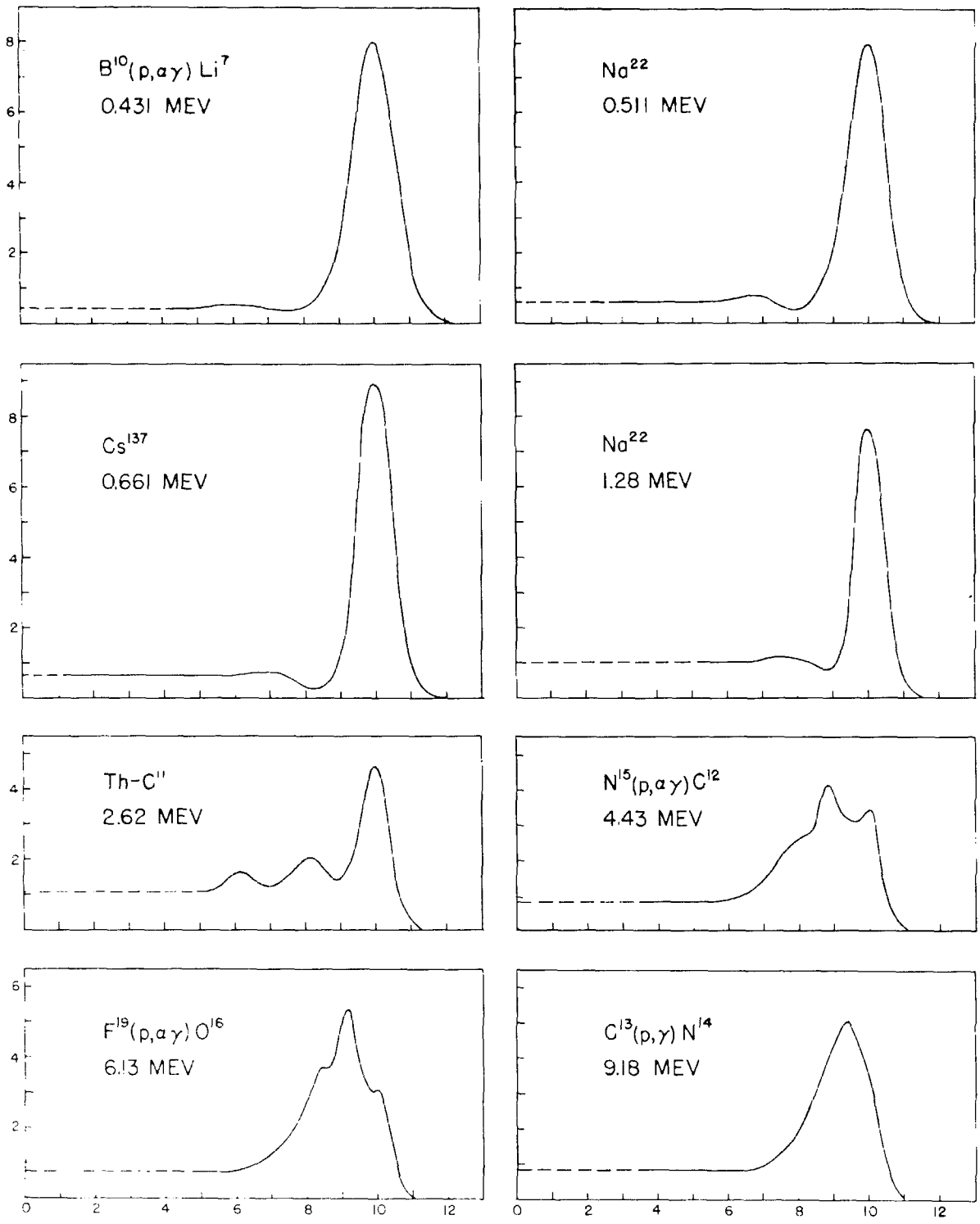
$B^{10}(p,\alpha\gamma)\,Li^{7}$
0.431 MEV
Na^{22}
0.511 MEV
Cs^{137}
0.661 MEV
Na^{22}
1.28 MEV
Th-C''
2.62 MEV
$N^{15}(p,\alpha\gamma)\,C^{12}$
4.43 MEV
$F^{19}(p,\alpha\gamma)\,O^{16}$
6.13 MEV
$C^{13}(p,\gamma)\,N^{14}$
9.18 MEV
0
2
4
6
8
10
12

FIG. 27

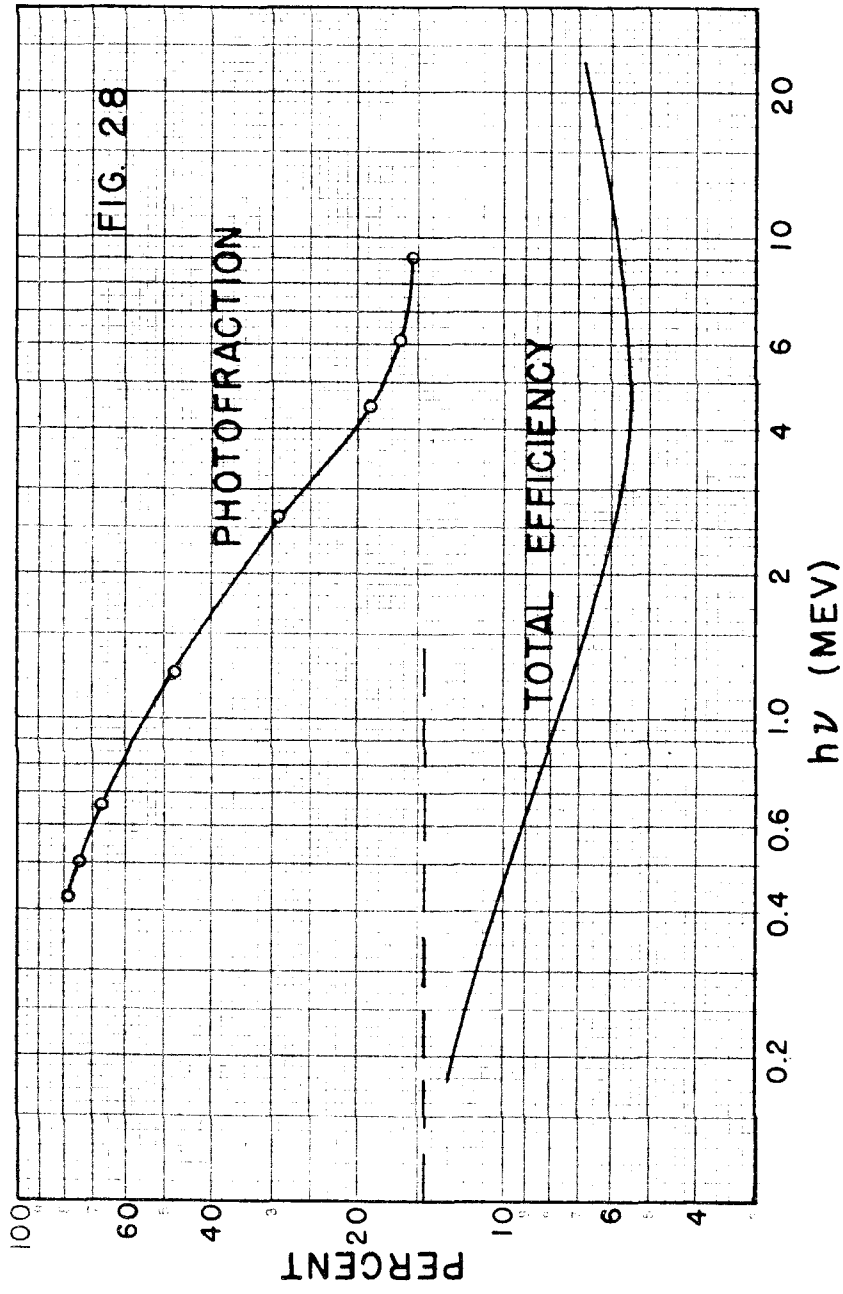
FIG. 28
PHOTOFRACTION
TOTAL EFFICIENCY
PERCENT
100
60
40
20
10
6
4
0.2
0.4
0.6
1.0
2
4
6
10
20
hν (MEV)